WSRC-TR-2003-00339, REVISION 0
SRT-RPP-2003-00207, REVISION 0

Key Words:
Hanford River Protection Project
Hanford Waste Tanks

Retention:
Permanent

Key WTP R&T References:
Task Specification:
24590-WTP-TSP-RT-01-025
Task Plan: WSRC-RP-2002-00429
Test Exception:
24590-WTP-TEF-RT-03-016
R & T Focus Area: Stream Integration
Scoping Statement: S-115

HIGH LEVEL WASTE LAG STORAGE AND FEED BLENDING

Mark J. Barnes, Savannah River Technology Center
David J. Sherwood, Washington Group International
C. Daniel Barnes, Savannah River Technology Center
Thomas B. Edwards, Savannah River Technology Center

NOVEMBER 2003

Westinghouse Savannah River Company
Savannah River Site
Aiken, SC 29808

Prepared for the U.S. Department of Energy Under Contract Number DE-AC09-96SR18500

SRS savannah river site ™

This page was intentionally left blank

TABLE OF CONTENTS

LIST OF FIGURES

LIST OF TABLES

This page intentionally left blank.

ABSTRACT

The Office of River Protection Hanford Waste Treatment and Immobilization Plant consists of three primary facilities: a Pretreatment Facility and two facilities for low-activity and high-level waste vitrification. The Pretreatment Facility contains unit operations which receive waste feed from the Hanford Tank Farms and separate it into two treated waste streams: a low-activity, liquid waste stream stripped of most solids and radioisotopes (processed through the Low-Activity Waste Vitrification Facility) and a high-level waste slurry containing most of the solids and radioisotopes (processed through the High-Level Waste Vitrification Facility). Blending of the later solids and radioisotopes streams and their resulting properties is the subject of this report. These mixtures are shown to be unreactive and pumpable by using statistically designed combinations of nonradioactive simulants for the process streams. Properties of the mixtures are also predicted numerically (with the Environmental Simulation Program) and compared with the experimental results. The results did not reveal any problematic solutions, properties, or conditions. The high viscosity and yield stress of the simulated sludge and the resulting test mixtures that included it are, however, of note.

This page intentionally left blank.

1.0 SUMMARY OF TESTING

SRTC performed small-scale tests to determine the behavior associated with blending streams in the High-level Waste (HLW) Lag Storage and Feed Blending Process System for the Hanford Waste Treatment and Immobilization Plant (WTP). The work reported here was planned and designed per References [1] and [2], respectively, in response to the Test Specification, Reference [3].

1.1 OBJECTIVES

The Task Specification [3] addresses activities for assessing waste stream mixing in the HLW Lag Storage and Feed Blending System vessels and the Plant Wash and Disposal System vessels. The HLW Lag Storage and Feed Blending System vessels accumulate mixtures of ion exchange eluate, and washed solids from the Ultrafiltration Process. Plant Wash and Disposal System vessels store solutions from cleaning, flushing, and decontamination processes.

Task activities addressing these two systems were divided into two parts. Previous work focused on the Plant Wash and Disposal System vessels (the front end of the Pretreatment Facility). This work has been described in Reference [4]. The work reported in this document addresses stream blending within the HLW Lag Storage and Blending System (i.e., the back end of the Pretreatment Facility).

The objective of this task is to determine how ion exchange eluate and Ultrafiltration Process washed solids interact. Specifically, identify changes in physical properties and possible chemical reactions. The work met all goals of the task. Work covered in this task produced the following:

- A test matrix showing mixtures of process streams for the HLW Lag Storage and Feed Blending System during the initial WTP feed sequence
- Experimentation with mixtures from these matrices, producing data such as:
  - Measurements of initial viscosity
  - Measurements of final (i.e., after 1 month) viscosity
  - Visual observations over a period of one month to detect any changes in solution turbidity. Changes in turbidity were not detected due to the starting appearance of the mixtures (i.e., all mixtures were highly opaque and registered a maximum measurable turbidity value greater than 1000 ntu from the outset of testing).

  - Observations of solution appearance, noting changes in consistency, color, solids content, and degassing
  - Measurements from isolating and characterizing solids which formed in the solution mixtures
  - Measurements of redox potential over a period of one month
  - Measurements to discern or quantify interesting, unusual, and unexpected behavior of the mixtures
- Comparison of experimental results with mathematical model simulations
- Assessment of what this information means to operation of the Pretreatment Facility
- Recommendations for improved design/operation of the Pretreatment Facility

1.2 CONDUCT OF TESTING

The scope of this task was to investigate the interaction of ion exchange eluates and ultrafiltration washed solids, specifically, focusing on changes in physical properties and chemical interactions. Originally, the Task Plan called for testing with all envelopes of waste, however, limited availability of both actual waste and characterization data for simulants limited this testing (Test Exception, 24590-WTP-TEF-RT-03-016). Also, the Task Plan and Specification included the blending of technetium eluate. The current flowsheet no longer includes technetium ion exchange and eluate, so it was removed from this testing (Test Exception, 24590-WTP-TEF-RT-03-016).

Simulant testing, using a statistically designed test matrix, was conducted using simulated AZ-102 sludge, simulated AN-102 Sr/TRU precipitate, and a typical simulated cesium concentrate. The task also included radioactive testing, with plans calling for using AY-102 sludge, AN-107 Sr/TRU precipitate, and AW-101 cesium concentrate. The unavailability of radioactive sludge forced the radioactive testing to be moved to another work scope (Scoping Study S-68) for completion at at a later time. Therefore, radioactive testing is not covered in this document. Nevertheless, physical properties of the sludge stored in the Hanford Tank Farms provided by the operating contractor is reviewed.

One set of experimental tests was conducted to map the variation of streams involved in the HLW Lag Storage and Feed Blending Process System. The nonradioactive testing used a statistically designed test matrix to vary the ratios of sludge, Sr/TRU precipitate, concentrated cesium eluate, and spent ion exchange resin.

Experimental details are elaborated upon in the next section. Typically, the experimental approach involved mixing (150 mL) test volumes of the appropriate waste simulants reflecting these streams and their nominal volumes. Where available, the waste simulants and samples used in the tests were obtained from other RPP task activities underway at SRTC. Upon blending of the simulants, chemical and physical properties of the mixtures were obtained over a period of one month. After completing 30 days of agitation, the mixtures were analyzed. Results were evaluated as to their potential for adversely affecting Pretreatment Facility operations. Test results were statistically evaluated and provided the following results:

- Measurements of physical and chemical property changes for these solutions (e.g., changes to the waste that could impact WTP operations such as changes in viscosity, yield stress, gassing, and exothermic reactions).
- Qualitative and quantitative analysis of reaction products from the mixtures. Further characterization of non-crystalline phases (e.g., scanning electron microscopy) or crystalline phases (e.g., powder X-ray diffraction) were performed. No significant gas formation was observed in the mixtures.

The results were assessed against numerical predictions of solution mixture behavior made with the most recent version of the *Environmental Simulation Program* available from OLI Systems, Inc. (Morris Plains, New Jersey).

1.3 RESULTS AND PERFORMANCE AGAINST OBJECTIVES

The objective of this task was to determine how ion exchange eluate and Ultrafiltration Process washed solids interact. Specifically, testing sought to identify changes in physical properties such as viscosity and yield stress, formation of gasses, increases in temperature, and chemical reactions. The work met all goals of the task except radioactive testing for verification purposes. This was transferred to a later program to be completed when radioactive sludge becomes available.

Testing with a limited set of nonradioactive simulants did not exhibit significant changes in the test slurries. The slurries were highly viscous and difficult to work with. Concentration of the sludge feed was extremely difficult. However a decrease in both viscosity and yield stress was observed from the start of testing to the end of testing with this limited set of simulants. This decrease signifies that processing of these slurries may become easier with increased mechanical processing.

Analysis of the test solids indicated that they were largely composed of aluminum- and iron-based oxides (as expected). Measurement of various solution parameters, such as viscosity and yield stress, showed that the simulant nonradioactive blends appeared devoid of problems. In addition, monitoring the solutions over 30 days demonstrated that the test blends reached near steady state condition almost immediately, and afterward remained relatively stable. No problematic conditions were identified. Statistical analysis demonstrated that a good correlation did exist between stream contribution (i.e., volume percent) and solids formation. An equation of fit was obtained for the three primary streams.

The use of the *Environmental Simulation Program™ (ESP)* from OLI Systems, Inc., to model the blended streams proved less useful. The accuracy of the program was hindered by the solution pH limitations of the software and the relative importance of solution pH on solids formation and resulting related physical properties in actual testing.

1.4 QUALITY REQUIREMENTS

The work described in this document was conducted in response to a Test Specification [3] and is described by the Task Plan [1] and subsequent experimental design documents [2]. The experimental program was performed to the NQA-1 standard.

This work was conducted in accordance with the WSRC Quality Assurance Program, which has been approved by WTP, and the WSRC Quality Assurance Management Plan (WSRC-RP-92-225). This program will apply the appropriate quality assurance requirements for this task from NQA-1-1989, and NQA-2a-1990, Part 2.7, as indicated by the QA Plan Checklist in Section VIII. RW-0333P QA requirements do not apply to this task (the work does not affect the quality of IHLW product). Experimentation in support of this task plan activity will not be used for assessing the performance of Important-to-Safety equipment.

Commercial computer software (e.g., Microsoft Excel or OLI Systems Software such as *Environmental Simulation Program*) was used for calculations. Software calculations were validated and verified by hand calculations. The Standards Laboratory calibrated all M&TE used in these experiments with the exception of meters used to measure pH, oxidation reduction potential, and turbidity. These were checked daily prior to use against standard solutions and gels. Calibration checks were performed daily.

This task did not generate data that will be used for environmental regulatory purposes. Therefore, per the "Quality Assurance Project Plan (QAPjP) for Testing Programs Generating Environmental Regulatory Data," PL-24590-QA00001, Rev. 0, the quality control for analytical data specified in the aforementioned QAPjP are not applicable. The determination of the non-applicability of this work for environmental regulatory purposes and the approach to institute quality controls as specified below was agreed to by the RPP-WTP customer (Washington Group International).

Analyses provided by SRTC's Analytical Development Section (ADS) were performed on a Routine QA/QC level. Routine Level is for general R&D support. ADS maintains a written method or instrument procedure for all Routine Level analyses. Quality Control is addressed through ADS's Measurement Control Program (MCP) for analytical services. Quality Control data are routinely tracked and evaluated. The ADS Quality Control program tracks long-term system performance of the Measurement Systems. These systems include instruments, standards and personnel (laboratory technicians and chemists). These records are available and auditable, but are not provided with sample analysis results. Laboratory notebook records comply with WSRC/SRTC procedures (L1 Manual) and include information requested by the Test Specification [3].

1.5 ISSUES

Assessment of the results obtained from testing did not yield any recognizable problematic solutions, properties, or conditions. The high viscosity and yield stress of the simulated sludge and the resulting test mixtures that included it are of note.

This page intentionally left blank.

2.0 CONDUCT OF EXPERIMENTAL PROGRAM

2.1 THE PRETREATMENT FACILITY

The Pretreatment Facility of the Hanford Waste Treatment and Immobilization Plant receives radioactive liquid waste from underground storage tanks in the Hanford Tank Farms: the slurry of material is called waste feed. Pretreatment Facility operations concentrate (or dilute, as required) this waste feed, separate radionuclides from it, and remove chemicals which adversely affect the vitrified product. The waste feed is categorized as:

- low-activity waste (LAW) - Envelope A, B, or C
- high-level waste (HLW) - Envelope D

Waste envelopes are defined in Table 2-1. Waste will be fed to the Pretreatment Facility one envelope at a time in the sequence shown by Table 2-2 and Figure 2-1.

The Pretreatment Facility can receive LAW in the Waste Feed Receipt Vessels (FRP-VSL-00002A/B/C/D); these tanks are interconnected and have a total capacity of 1.5 M gal (5680 m^3). These tanks also receive recycle streams from the Pretreatment Facility. Envelope D HLW feed is the sludge at the bottom of some Hanford tanks, for example:

- AZ-101 and AZ-102
- SY-102
- AY-101 and AY-102
- AW-103 and AW-104
- C-104, C-105, and C-106

The sludge layer is where most of the actinides and fission products reside. HLW feed will generally be diverted from the Waste Feed Receipt Vessels to the HLW Feed Receipt Vessel in 160,000-gal (606 m^3) batches. Envelope D also consists of separations products from Pretreatment Facility operations which remove solids from Envelopes B and C waste feed and radionuclides separated from Envelopes A, B, and C. These three LAW envelopes largely consist of supernate, and this aqueous material holds large amounts of the dissolved radionuclides ^{137}Cs and ^{99}Tc.

Waste feed received from the Hanford Tank Farms by the Pretreatment Facility will have a five molar sodium concentration. Such a high specific gravity means that evaporation is not required before the stream is sent to Pretreatment Facility separations processes. Waste feed in the Waste Feed Receipt Vessels will therefore generally be routed directly to the Ultrafiltration Process System and not the Waste Feed Evaporation Process System.

The volume of the vitrified product increases with increasing sodium in the waste. Solids from LAW Feed Envelopes A and B and HLW Feed Envelope D will be collected in a slurry by the Ultrafiltration Process and washed in dilute caustic to reduce the sodium concentration. Strontium and transuranics (TRU) must be precipitated from LAW Feed Envelope C first; then this slurry will be washed as well.

Sulfates, which affect glass processing, will also be removed by the washing operation in the Ultrafiltration Process. This process also features a caustic leaching operation after the (dilute caustic) washing operation. Caustic leaching will remove a large fraction of aluminates and significant amounts of phosphates and chromium compounds from the waste feed. Radionuclides such as ^{137}Cs and ^{99}Tc will be washed away from the sludge by the Ultrafiltration Process. Cesium will be separated from the process effluent by subsequent ion-exchange operations. Recycle streams are produced by the Pretreatment Facility and the LAW and HLW Vitrification Facilities; these streams route to the Pretreatment Facility for processing with the waste feed or disposal to the Hanford Liquid Effluent Retention Facility (LERF).

Table 2-1. Definition of Waste Feed Envelopes for the Hanford WTP

Waste Feed*	**Sodium Content, [Na], moles/liter**
Envelopes A, B, C	4 – 10
Envelope B: 241-AZ-101 and 241-AZ-102 Supernatant	2 – 5
Envelope D: HLW Slurry and other HLW Liquids	0.1 – 10
Hanford Tank waste is categorized as Envelope A, B, C, or D. Envelopes A and C are LAW: Envelope A waste contains only entrained solids and Envelope C contains these as well as radioisotopes in compounds which will be precipitated from solution. Envelope D is HLW with large amounts of undissolved solids. Envelope B waste feed contains a LAW fraction (supernate) and a HLW fraction as undissolved solids; LAW supernate from a tank with this type of waste is designated Envelope B, while the HLW fraction is designated Envelope B/D.	
Low-Activity Waste Feed • LAW feed may contain up to two weight percent solids. Solids are defined as the product of centrifuging LAW feed, separating and then drying the solids, and finally removing the dissolved solids fraction. • LAW feed shall not contain a visible separate organic phase. • LAW feed generates gases such as hydrogen, nitrogen, nitrous oxide, and methane, and also contains ammonia. • LAW feed shall have $[^{137}Cs] \leq 1.2$ curies/liter. • Waste feed from tanks 241-AZ-101/102 shall have $[^{137}Cs] \leq 3.0$ curies/liter.	
High-Level Waste Feed • The HLW slurry will contain a mixture of liquids (Envelopes A, B, or C) and solids (Envelope D). For liquid fractions less than three molar sodium, the liquid shall be treated as if it were three molar sodium. • The feed concentration will be between 10 and 200 grams of unwashed solids/liter, except for waste feed from tanks 241-AZ-101/102, where minimum solids content does not apply. • Compositions for Envelope D unwashed solids are defined in terms of elemental or anion concentrations and radionuclide activities per 100 grams equivalent non-volatile waste oxides. The non-volatile waste oxides include sodium oxide and silicon oxide. • The HLW waste feed will not contain a visible organic layer.	

*A slurry is a pumpable material comprised of liquid and solid fractions.

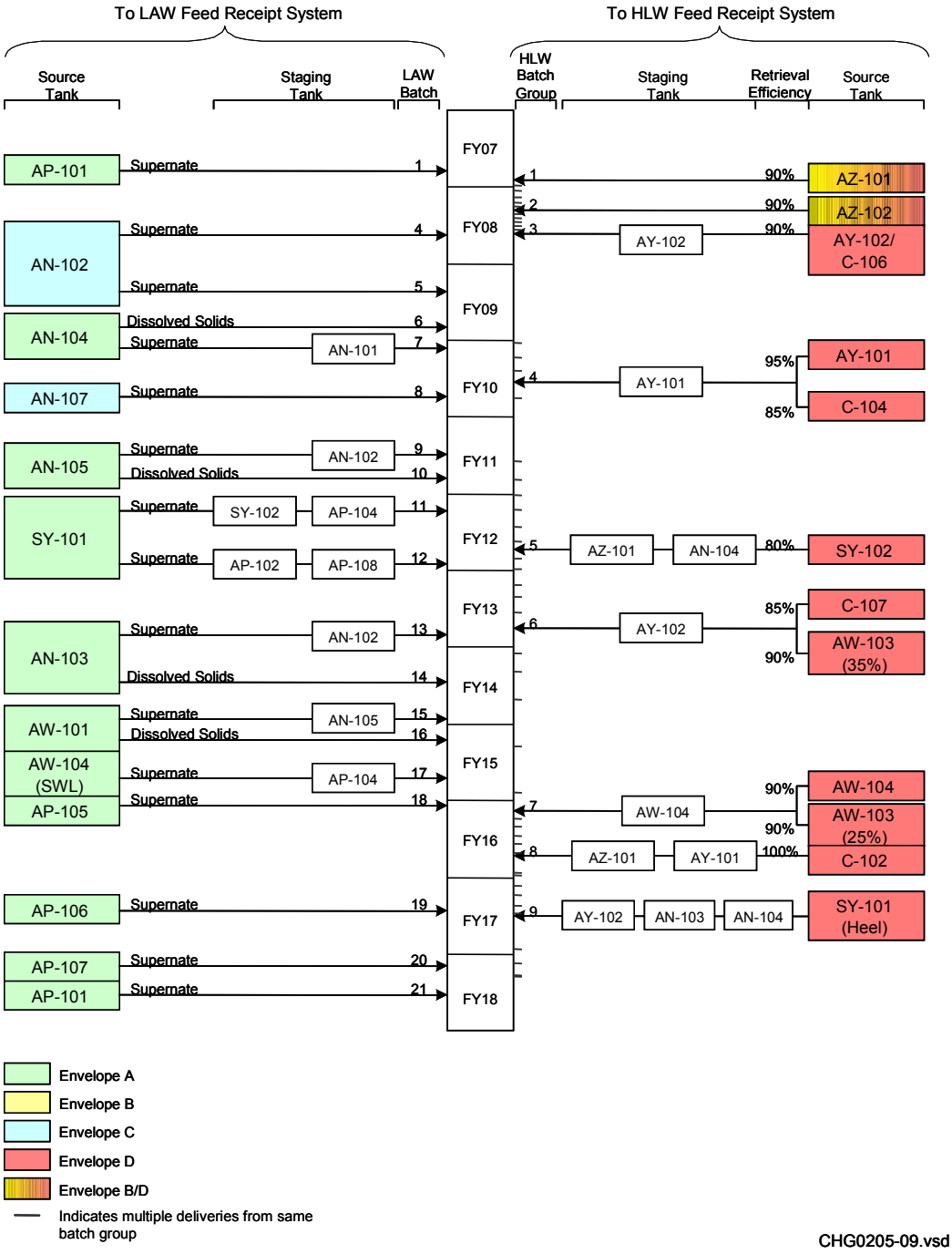

Figure 2-1. Time-Phased Delivery of Waste from Tank Farms to Hanford Waste Treatment and Immobilization Plant

(Taken from River Protection Project System Plan, Rev. 0, ORP-11242, July 2002. Note that this sequence has been altered since it was originally issued.)

Table 2-2. Initial Waste Feed Staging Sequence

Envelope	Source Tank	Waste Type	Staging Tank	Batch
A	241-AP-101	Supernate	Self	1
B	241-AZ-101	Supernate/Sludge	Self	2
	241-AZ-102	Supernate/Sludge	Self	3
C	241-AN-102	Supernate	Self	4
			Self	5
A	241-AN-104	Supernate/Solids	Self	6
			241-AN-101	7
C	241-AN-107	Supernate	Self	8

The Waste Feed Evaporation Process System will receive the recycle streams requiring processing and concentrate them to five molar sodium. The concentrated recycle stream will be routed back to the Ultrafiltration Process System. The Pretreatment process separates waste feed from the Hanford Tank Farms into two process streams:

- **treated LAW stream** obtained by stripping off solids (by the Ultrafiltration Process) and radionuclides (with the Cesium and Technetium Ion Exchange Processes) from the waste feed stream
- **blended HLW stream** comprised of the solids-rich slurry (from the Ultrafiltration Process) mixed with two concentrated, radioisotope-bearing (eluate) process streams (from the Cesium and Technetium Ion Exchange Processes).

The treated LAW stream will, in the final Treated LAW Evaporation Process, be concentrated up to the solids crystallization point (8 to 10 molar sodium). The final blended HLW stream will not be concentrated. This treated LAW stream will be sent to the LAW Vitrification Plant where it will be concentrated in a boro-silicate glass form. The blended HLW stream will contain most of the radioactive strontium, cesium, and transuranics (TRU - alpha-emitting radionuclides with atomic numbers greater than 92 and half-lives longer than 10 years). It will be sent to the HLW Vitrification Plant to be concentrated in another boro-silicate glass form.

Figure 2-2 provides a broad overview of the Pretreatment process for the WTP under the nominal operating conditions in effect when this Task was planned. The Pretreatment Facility uses the following systems for receiving waste feed, concentrating waste feed and recycle streams, stripping solids and radioisotopes from the waste feed, blending the solids and radioisotopes into HLW product, concentrating purified LAW liquors, and storing the HLW and LAW product streams:

- Waste Feed Receipt Process (FRP)
- Waste Feed Evaporation Process (FEP)
- Ultrafiltration Process (UFP)
- Plant Wash and Disposal (PWD); Radioactive Liquid Waste Disposal (RLD)
- HLW Lag Storage and Feed Blending Process (HLP)
- Cesium Ion Exchange (CXP)
- Treated LAW Evaporation Process (TLP)
- Treated LAW Concentrate Storage Process (TCP)

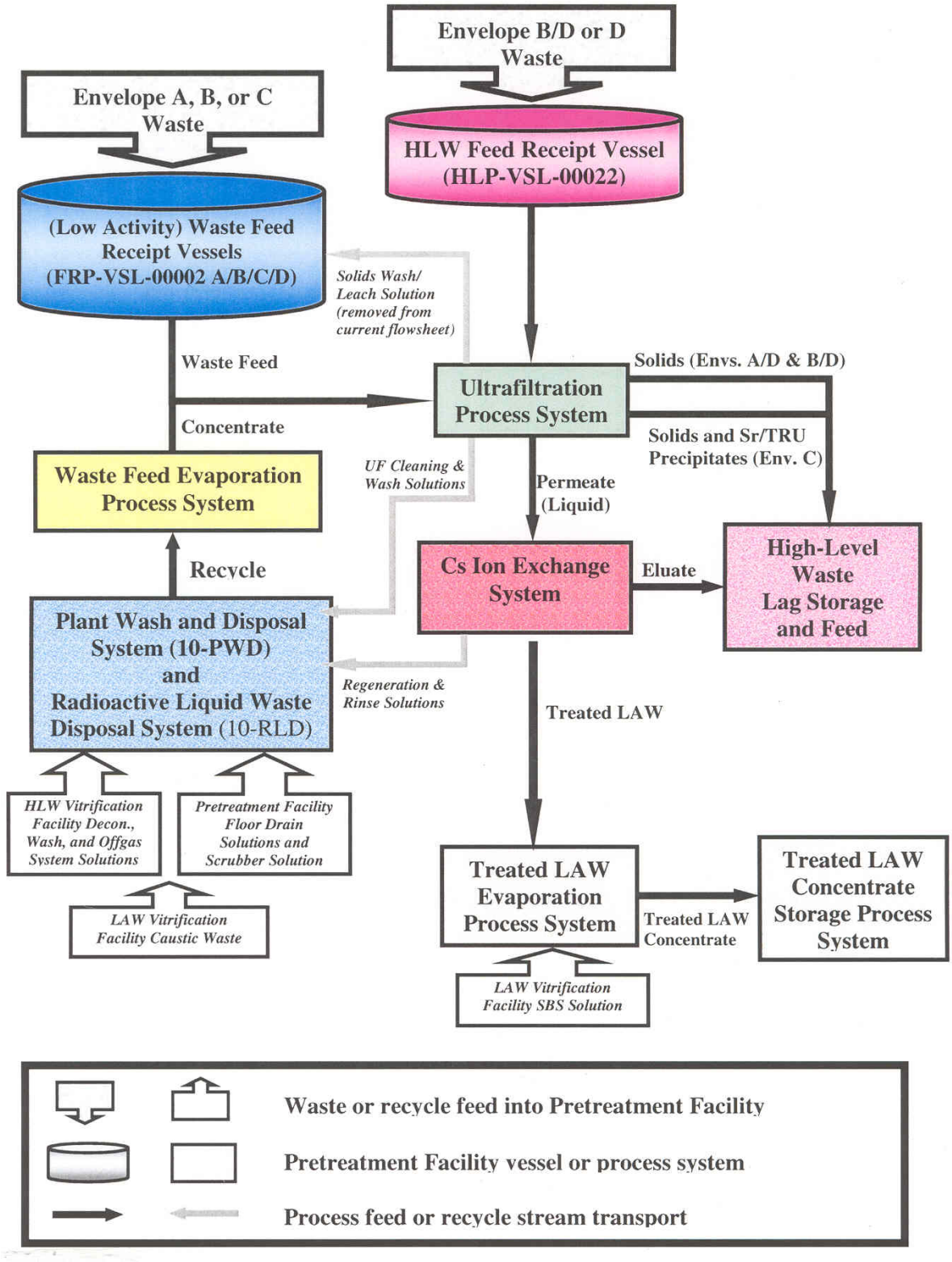

Figure 2-2. Schematic of Pretreatment Facility Process Flow

Pretreatment Facility processes must be able to accommodate a variety of waste streams mixing together. Changes to the waste that could impact WTP operations include increased viscosity and shear strength, precipitation of solids, gel formation, foaming, gassing, and exothermic reactions.

2.2 SELECTION OF SOLUTIONS AND MIXTURES

The HLW Lag Storage and Feed Blending Process is the terminal storage system for all treated HLW streams in the Pretreatment Facility. The next process for the material collected in this system is the HLW Vitrification Facility. The HLW Lag Storage and Feed Blending System receives and stages pretreated process slurries of HLW solids and Sr/TRU precipitates from the Ultrafiltration Process and mixes them with Cs eluate concentrates from the cesium ion exchange process. Output from Ultrafiltration is 20 wt. % solids for Envelopes A/D and B/D and 15 wt. % for Envelope C/D. Two HLW Lag Storage vessels (HLP-VSL-00027A/B) feed the HLW Feed Blending Vessel (HLP-VSL-00028). Treated HLW solids are combined there with concentrated Cs eluate from CNP-VSL-00002. HLP-VSL-00028 may also receive off-specification ion exchange resin (including Cs/Sr slurry). Figure 2-3 shows a schematic of the HLW Lag Storage and Feed Blending Process System.

Originally, the Task Plan included the blending of technetium eluate as a stream in the system. However, the current flowsheet no longer includes technetium ion exchange and eluate, so it was removed from this testing (per guidance of Reid Peterson, Test Exception 24590-WTP-TEF-RT-03-016 dated March 21, 2003). Based on discussions with WTP Research and Development personnel, it was determined that simulant testing would utilize simulated AZ-102 sludge, simulated AN-102 Sr/TRU precipitate, and a typical simulated cesium concentrate.

2.3 EXPERIMENTAL TEST DESIGN

The statistical design for nonradioactive simulant testing of the streams relevant to this study was developed from discussions with Reid Peterson and follow-up correspondence with David Sherwood and Mike Boh. The bounding flowsheet throughputs set the minimum and maximum flowrates for the streams.

- One batch (81000 gallons) of HLW Lag (sludge and Sr/TRU precipitate) in either 30 days or 60 days
- One batch (1500 gallons) of cesium concentrate every 30 days

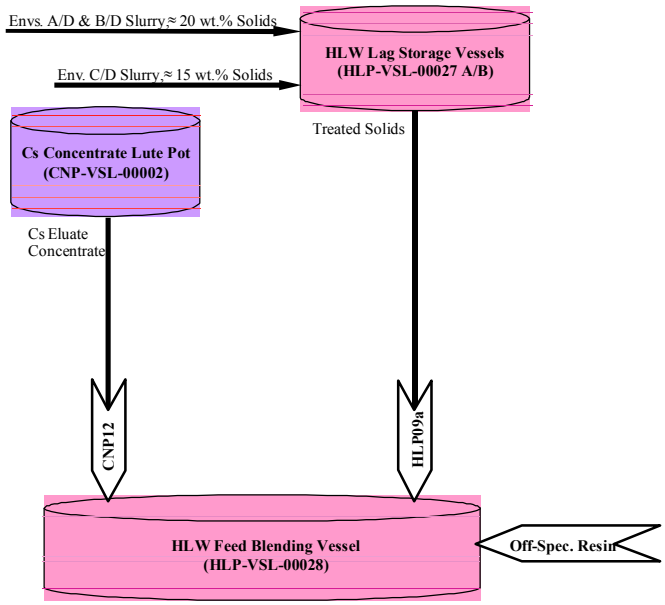

Figure 2-3. Schematic of the HLW Lag Storage and Feed Blending Process System

The minimum volume fraction for HLW lag and maximum volume fraction for cesium concentrate assumes one batch of HLW lag and two batches of cesium concentrate are blended. The maximum volume fraction for HLW lag and minimum volume fraction for cesium concentrate assumes one batch of HLW lag and one batch of cesium concentrate are blended. Table 2-3 provides the minimum and maximum volume fractions based upon these flowrates. The minimum (and also nominal) flowrate for the off-specification ion exchange resin stream was set at 0 due to the non-routine nature of the stream. Given the speculation concerning the off-specification resin stream, the majority of the tests did not include resin. However, a few tests were planned to simulate the presence of up to 400 gallons (0.35 volume %) of off-specification resin added to the HLW Feed Blending Vessel (a tank with a working volume of 115,000 gallons). As part of the design, the sludge: TRU precipitate ratio was tested at 3 levels, namely 90:10, 95:5, and 100:0.

Table 2-3. Minimum and Maximum Volume Fractions of Waste Stream Influents to the HLW Feed Blending Vessel (HLP-VSL-00028)

Stream	Minimum Volume Fraction	Maximum Volume Fraction
HLW Lag Storage Washed Solids (HLP09a)	0.9643	0.9818
Cs Eluate (CNP12)	0.0182	0.0357
Off Specification Ion exchange resin	0.00	0.0035

The Statistical Consulting Section (SCS) of SRTC provided a statistical design for nonradioactive testing to examine the varying composition in the HLW Feed Blending Vessel (HLP-VSL-00028) using the maximum and minimum volume fractions identified above. The design, conditions, and assumptions that the design is based upon are provided in Appendix A. In summary, the design from Appendix A, shown below in Table 2-4, calls for 14 tests where the only parameter is the varying contribution from the influent streams. The design varies within the bounding volume fractions provided in Table 2-3. The design includes duplicate tests to provide a measure of the repeatability of the experimental process and associated analytical procedures.

Table 2-4. Nonradioactive Statistical Test Design

Description	Trial ID	HLW Lag (vf)	HLW Lag sludge (vf)	HLW Lag TRU (vf)	Cs Conc (vf)	Off-Spec Resin (vf)
HLW lag is sludge only.	FB01	0.96430	0.96430	0.00000	0.03570	0.00000
	FB02	0.98180	0.98180	0.00000	0.01820	0.00000
	FB03	0.97305	0.97305	0.00000	0.02695	0.00000
HLW lag: 95% sludge and 5% TRU.	FB04	0.96430	0.91609	0.04822	0.03570	0.00000
	FB05	0.98180	0.93271	0.04909	0.01820	0.00000
	FB06	0.97305	0.92440	0.04865	0.02695	0.00000
HLW lag: 90% sludge and 10% TRU	FB07	0.96430	0.86787	0.09643	0.03570	0.00000
	FB08	0.98180	0.88362	0.09818	0.01820	0.00000
	FB09	0.97305	0.87575	0.09731	0.02695	0.00000
Runs spiked with off-spec resin stream	FB10	0.96955	0.96955	0.00000	0.02695	0.00350
	FB11	0.96955	0.87260	0.09696	0.02695	0.00350
Duplicate runs for reproducibility	FB12	0.97305	0.97305	0.00000	0.02695	0.00000
	FB13	0.97305	0.87575	0.09731	0.02695	0.00000
	FB14	0.97305	0.92440	0.04865	0.02695	0.00000

vf = volume fraction

2.4 EXPERIMENTAL TEST METHOD

2.4.1 Simulant Preparation and Characterization

Four Lag Stream and Feed Blending simulants were required for the test design. The objective for the simulants was to obtain them from other concurrent testing at SRTC. Simulants of two of the four streams were available: simulated AN-102 Sr/TRU precipitate and simulated AZ-102 cesium eluate concentrate. The third (and largest contributing stream) simulant was prepared especially for this program since an insufficient quantity existed. The fourth simulant was spent ion exchange resin. Caustic-treated fresh SuperLig® 644 resin was used for this purpose. All simulants were nonradioactive. When required, personnel prepared simulant solutions from reagent-grade chemicals using calibrated balances checked daily before use. The weights used for balance checks received calibration by the SRTC Standards Laboratory. The accuracy of glassware used to measure volumes was previously verified by gravimetric methods using water as a standard. Temperature measurements used equipment calibrated by the SRTC Standards Laboratory. All M&TE used in this task received calibration or verification for accuracy prior to their use.

The AN-102 simulant was obtained from Michael Poirier (Scoping Study S-43). The salt solution simulant preparation and resulting filtration and characterization are described in Reference [5]. The material obtained has been designated as Batch AN102R2. The precipitate material was not washed or concentrated at the time it was obtained. Under the direction of Michael Poirier, the solids were to be washed (an equal volume wash was attempted) and concentrated to 15 wt % solids. Unfortunately, during the process, the filtration unit experienced mechanical failure leaving the solids only partially washed and concentrated. Concentration to 15 wt % was completed on a smaller sub-batch. No further washing was attempted. Photographs of the concentrated precipitate are shown in Figure 2-4. Chemical characterization of the final material is provided in Appendix B. Rheological measurements of the feed material are contained in Appendix C. X-ray diffraction patterns of the stock AN-102 precipitate are contained in Appendix D.

The simulated AZ-102 cesium eluate concentrate was obtained from Robert Pierce (Scoping Study S-78). Preparation and characterization of the concentrated cesium eluate simulant has been described in Reference [6]. The material used in this test program was from Pierce's Experiment # 2. The solution contained minimal solids. Photographs of the eluate are shown in Figure 2-5. 100 mL of the eluate concentrate was neutralized with 25.8 mL of 19 M NaOH prior to use. Characterization of the final material is provided in Appendix B. Rheological measurements of the feed material are contained in Appendix C.

Caustic treated SuperLig® 644 ion exchange resin (Lot # I-D5-03-06-02-35-60, *IBC Advanced Technologies*, American Fork, Utah) was used to simulate spent ion exchange resin. The resin was obtained from Charles Nash in its hydrogen form and had not been used prior to this work. It was caustic treated prior to its use by overnight exposure to dilute NaOH. Chemical characterization of the final material is shown in Appendix B. A photograph of the ion exchange resin is shown in Figure 2-6. Rheological measurements of the feed material are contained in Appendix C.

Side View Top View

Figure 2-4. Photographs of simulated AN-102 Sr/TRU Precipitate (15 wt %)

Side View Top View

Figure 2-5. Photographs of simulated AZ-102 Eluate Concentrate

Figure 2-6. Photograph of SuperLig® 644 Ion Exchange Resin

An insufficient quantity of simulated AZ-102 sludge was available from other programs. As a result, a new batch of sludge was prepared from an approved recipe developed by Russell Eibling and reported in Reference [7]. The sludge was concentrated using a crossflow filter. However, mechanical pump problems occurred during its concentration. At the direction of Project Personnel, concentration of the slurry was halted at 14.7 wt % (desired concentration was 20 wt % solids) in order to prevent further delays. Characterization of the final material is shown in Appendix B. Rheological measurements of the feed material are contained in Appendix C. Photographs of the simulated sludge solids are shown in Figure 2-7. X-Ray diffraction patterns of the simulated AZ-102 sludge are contained in Appendix D. Preparation instructions are provided in Appendix E.

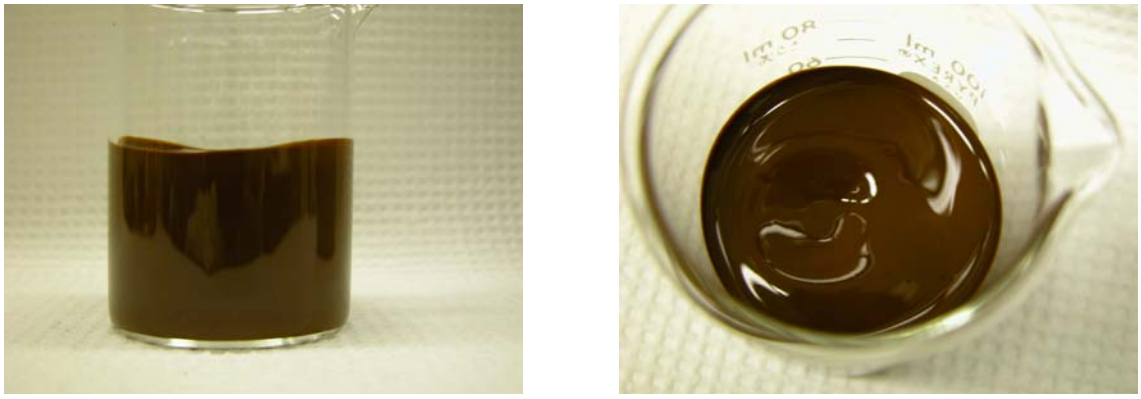

Side View **Top View**

Figure 2-7. Photographs of simulated AZ-102 sludge (14.7 wt % solids)

2.4.2 Test Protocol

The experimental approach for testing involved mixing, observation, and measurement of slurry properties of the test mixtures. Testing was conducted at 25 °C. Typical test volumes of 150 mL were sufficient to permit analysis and measurement. The test atmosphere was air. Upon blending of the simulants, chemical and physical properties of the mixtures were obtained with laboratory equipment available at SRTC. Tests were monitored weekly over 30 days. Testing included the following:

- Measurements of physical and chemical property changes for these solutions
- Qualitative and quantitative analysis of reaction products from the mixtures

2.4.2.1 Test Instructions

This section describes the test instructions provided to the technician during initiation of the tests.

1. Obtain the following test stock solutions:
   - Simulated AZ-102 sludge (14.8 wt %)
   - Simulated AN-102 Precipitate (15 wt %)
   - Neutralized AZ-102 cesium eluate (concentrated)
   - Caustic treated Cesium ion exchange resin

2. These instructions cover the initiation of 14 tests. All 14 tests are similar except for the volume of stock materials that will be used in each test. Instructions are provided below for the first test and an Additions Table (Table 2-5) is also provided to detail the volumes to be used for all 14 tests. Repeat the instructions in Steps 3 to 19 for all 14 tests.
3. Measure out the required volume of Simulated AZ-102 Sludge. Record the exact volume used.
4. Place the material in a 200 (or 250 mL) beaker. Add a stirbar and stir.
5. Measure out the required volume of Simulated AN-102 Precipitate. Record the exact volume used.
6. Add it to the test beaker while stirring.
7. Measure out the required volume of Simulated, Neutralized AZ-102 Cesium Eluate. Record the exact volume used.
8. Add it to the test beaker while stirring.
9. If required, measure out the quantity of ion exchange resin. Record the exact volume used.
10. Add it to the test beaker while stirring.
11. Record the appearance of the resulting solution and any notable observations.
12. Make a note if gas evolution was observed and level of significance if observed.
13. Record the maximum temperature observed.
14. Record the final solution pH.
15. Record the redox potential (ORP) of the final mixture.
16. Photograph the solution.
17. Transfer a portion of the mixture to a turbidity tube and measure the turbidity.
18. Transfer the solution (including the turbidity portion) into a 250-mL PE bottle (pre-labeled).
19. Remove 50 mL of the test solution and place in a separate PE bottle and set aside for viscosity analysis by ITS.
20. Place all 250 mL test bottles in the shaker oven at 25 °C.
21. Each week (every seven days) measure the turbidity, pH, ORP, and photograph each test solution. Make a note of any changes in appearance of each test solution. Replace the solutions in their original test bottles and resume continuous shaking at 25 °C.
22. The tests will run for a minimum of 30 days.

Table 2-5. Additions Table - What Volumes to Mix

Test ID	AZ-102 Sludge (mL)	AN-102 Precipitate (mL)	Concentrated Cesium Eluate (mL)	Ion Exchange Resin (mL)
FB01	144.6	0.0	5.4	0.0
FB02	147.3	0.0	2.7	0.0
FB03	146.0	0.0	4.0	0.0
FB04	137.4	7.2	5.4	0.0
FB05	139.9	7.4	2.7	0.0
FB06	138.7	7.3	4.0	0.0
FB07	130.2	14.5	5.4	0.0
FB08	132.5	14.7	2.7	0.0
FB09	131.4	14.6	4.0	0.0
FB10	145.4	0.0	4.0	0.5
FB11	130.9	14.5	4.0	0.5
FB12	146.0	0.0	4.0	0.0
FB13	131.3	14.6	4.0	0.0
FB14	138.7	7.3	4.0	0.0

2.4.3 Analytical Methodology

Filtrate samples were obtained with a syringe fitted with a 0.45µ Nylon syringe filter disc. Solids were obtained by vacuum filtering a portion of the sample through a 0.45µ Nylon filter disc. Collected solids were washed to remove interstitial supernate. Samples of the solids fraction were prepared for analysis by fusion with sodium peroxide followed by uptake in hydrochloric acid. A list of analytical methods used to characterize solutions and their abbreviations used throughout this document is provided in Table 2-6.

Table 2-6. Analytical Methods Used in Recycle Stream Testing

Analytical Method	Analyte	Abbreviation
Ion Chromatography	NO_3^-, NO_2^-, SO_4^{2-}, Cl^-, F^-, HCO_2^-, $C_2O_4^{2-}$, PO_4^{3-}	IC
Titration	OH^-, total base, CO_3^{2-}	Titration
ICP-AES	multiple elements	ICP-ES
Scanning Electron Microscopy	Elemental	SEM
X-Ray Diffraction	Crystalline species	XRD

This page intentionally left blank.

3.0 EXPERIMENTAL RESULTS

3.1 SIMULANT FEED CHARACTERIZATION

Chemical analysis (see Appendix B) of the simulated AZ-102 sludge shows the solid phase consists primarily of aluminum and iron based compounds with compounds of manganese, cadmium, silicon and zirconium in lesser amounts. Trace metals are also observed in the solids. The supernate of the AZ-102 sludge is rather dilute (as a result of the washing phase of its preparation). X-ray diffraction of the sludge solids showed primarily aluminum and silicon based oxides; no discrete iron-containing phases were detected. Scanning electron microscopy was in agreement and showed the presence of significant amounts of iron, aluminum, oxygen, carbon, zirconium and cadmium. The simulated sludge was found to have a yield stress of 19.9 Pa and a viscosity of 7.92 cP.

The simulated AN-102 Sr/TRU precipitate solids contain large amounts of strontium, manganese, and sodium, as expected. Its supernate contains more salt than the AZ-102 sludge. The sodium concentration is about 3.6 M (as a result of the partial wash) with significant contribution from common anions such as nitrate, nitrite, and hydroxide. Analysis of the solids by XRD shows the presence of strontium carbonate, sodium nitrate, sodium oxalate, and sodium carbonate. Manganese was not detected. Scanning electron microscopy was in agreement and showed the presence of significant amounts of strontium, manganese as well as smaller amounts of sodium, sulfur, aluminum, and calcium. The simulated 15 wt % AN-102 precipitate had a small yield stress of 0.6 Pa and a viscosity of 4.85 cP.

The AZ-102 cesium eluate concentrate contained very little solids, so no solids analysis was performed. The composition of the concentrated eluate shows a high sodium content (6.2 M) that is essentially all sodium nitrate. The eluate solution was very dark, but transparent. Its color was a dark brown purple (depending on how light was applied to it). The solution exhibited no measurable yield stress (0 Pa) and its viscosity was 3.05 cP.

The supernate of the spent ion exchange resin (caustic treated SuperLig® 644) had a viscosity of 0.93 cP. The resin particles settled out of solution too fast to get a measure of the viscosity with the particles suspended. The resin had no measure yield stress (0 Pa). Chemical analysis was performed but little salts or metals were observed. An SEM of the resin showed the presence of sodium, aluminum, and silica.

3.2 EXPERIMENTAL TEST RESULTS

3.2.1 Physical Properties

Each of the 14 blended test solutions was monitored for over 30 days. There was little if any change in appearance of the test solutions. The only notable observation was that the solutions became more fluid with time. The large degree of solids present in the tests made it impossible to observe or measure small quantities of new precipitate (as was possible in blending studies of the various recycle simulants in scoping study S-113). All of the solutions looked very much the same. Their appearance looked exactly like that of the primary component - simulated AZ-102 sludge. Figure 3-1 provides photographs of both simulated AZ-102 sludge and Test FB01 for comparative purposes.

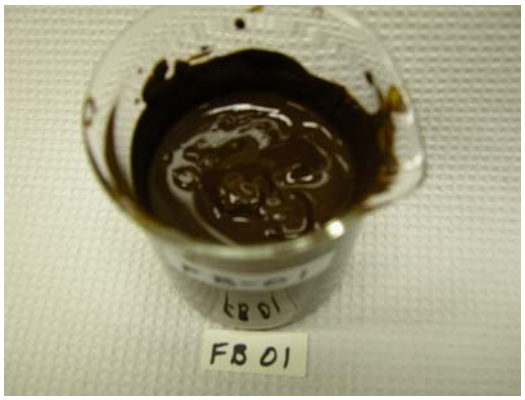

Test FB-01

Simulated ZA-102 Sludge

Figure 3-1. Photographs of Test FB-01 and simulated AZ-102 sludge

No significant gas evolution was observed upon blending or from week to week during testing. No gels formed and no thickening of the solution was noticeably evident upon mixing. Additionally, solution pH and redox potential were determined. The redox potential for the test solutions was difficult to measure. It was necessary to wait several minutes for the measurement to stabilize. Presumably, the highly viscous properties played a role in this observation. As expected, turbidity was greater than 1000 ntu for all tests from the start of testing. The maximum temperature change observed upon the initial blending was recorded (maximum of all tests was 1.2 °C). Viscosity was measured at both the start and end of the 30 days of testing (see Appendix F). Upon completion of the tests, the weight percent solids contained in the test solutions were determined. Data from these measurements are contained in Table 3-1 through Table 3-5.

Table 3-1. pH Values of Test Solutions

Test	Solution pH				
	Day 1	Week 1	Week 2	Week 3	Final
FB01	10.92	10.93	10.99	10.92	10.90
FB02	11.04	11.06	11.03	11.03	11.05
FB03	10.98	10.97	10.99	10.99	11.03
FB04	11.41	11.36	11.37	11.35	11.38
FB05	11.48	11.42	11.45	11.44	11.46
FB06	11.43	11.41	11.47	11.42	11.45
FB07	11.71	11.67	11.71	11.63	11.67
FB08	11.76	11.75	11.78	11.72	11.73
FB09	11.78	11.72	11.76	11.69	11.71
FB10	10.94	10.96	10.98	10.93	10.95
FB11	11.69	11.64	11.68	11.63	11.64
FB12	11.00	10.98	11.06	11.02	11.07
FB13	11.68	11.70	11.75	11.69	11.70
FB14	11.40	11.43	11.47	11.43	11.42

Table 3-2. Redox Potential of the Test Solutions

Test	Oxidation-Reduction Potential (mv)				
	Day 1	Week 1	Week 2	Week 3	Final
FB01	16	NA*	116	137	124
FB02	64	92	81	113	88
FB03	74	104	87	121	87
FB04	23	88	61	97	68
FB05	NA*	83	48	63	57
FB06	39	80	51	64	59
FB07	NA*	34	37	40	28
FB08	NA*	34	31	36	31
FB09	NA*	46	30	29	23
FB10	67	67	75	80	69
FB11	29	11	8	28	29
FB12	117	81	73	108	73
FB13	47	45	28	60	30
FB14	56	52	52	71	42
Standard[#]	484	483	483	482	481

*The measured value was determined to be inaccurate.
[#]A ferrous-ferric reference solution was used each day data was recorded. The potential of the platinum electrode for a Ag/AgCl/saturated KCl reference electrode in the ferrous-ferric reference solution at 25 °C is +475 mv. The slight deviation of the measured value from the reference value was deemed insignificant given differences in temperature and other experimental conditions.

The solution pH remained very stable throughout the month of testing. All tests had pH values near 11. The redox (or oxidation reduction) potential was much more troublesome than the solution pH. Typically, the solutions required more than 30 minutes for their measurement to stabilize, often times, it was difficult to determine when the reading had stabilized. As a result, a few measurements were determined to be inaccurate when assessed against readings from other weeks. All redox potentials were slightly positive. Nearly all were relatively stable indicating a steady state was reached fairly quickly (comparatively, in blending studies of recycle solutions in scoping study S-113, changes of several hundred millivolts were observed). The oxidation reduction potential measurement establishes the ratio of oxidants to reductants within a solution. The electropositive nature of the solutions reflects the ability to oxidize species in solution.

All 14 tests exhibited physical properties resembling the simulated AZ-102 sludge. This isn't surprising since it comprises between 87 and 98 percent (by volume) of the test solutions. The solids content in each solution measured between 14 and 15 wt %. The slight variations in measured solids concentration are due to the slight variation in sludge contribution and experimental error. For comparison, the simulated sludge was 14.7 wt %. Density of the test solutions ranged from 1.139 to 1.160 g/mL. The rise in temperature observed upon blending of the solutions was minimal and ranged from 0.3 to 1.2 °C.

Table 3-3. Physical Properties of Test Solutions

Test	Temperature Rise (°C)*	Solids (wt %)	Density (g/mL)
FB01	0.3	14.83	1.140
FB02	0.5	15.10	1.139
FB03	0.3	14.94	1.149
FB04	0.7	14.61	1.156
FB05	0.8	14.78	1.147
FB06	0.7	14.61	1.146
FB07	0.9	14.10	1.160
FB08	0.6	14.33	1.143
FB09	0.8	14.33	1.130
FB10	0.9	14.86	1.143
FB11	1.0	14.36	1.130
FB12	0.8	14.82	1.141
FB13	0.7	14.25	1.158
FB14	1.2	14.65	1.150

*Temperature rise calculated from room temperature (22.9 °C) and the highest measured temperature upon mixing of feed solutions.

The initial viscosity of the test solutions ranged from 7 to almost 10 cP. Again, the properties of the individual tests reflect the large contribution of simulated AZ-102 sludge (7.9 cp). The data appears to track with wt % solids concentration. After 30 days of almost continuous agitation, the viscosity had dropped to about 5 cP in every test. The change in viscosity was visually evident during testing. The slurries flowed more easily by the end of testing (see Figure 3-1 and Figure 3-2 for before and after testing photographs of two test solutions).

Table 3-4. Viscosity of Test Solutions

Test	Initial Viscosity (cP)	Final Viscosity (cP)	Change in Viscosity (cP)
FB01	9.69	5.34	-4.35
FB02	9.31	5.27	-4.04
FB03	9.55	5.22	-4.33
FB04	7.60	5.25	-2.35
FB05	8.67	5.15	-3.52
FB06	8.80	5.16	-3.64
FB07	7.60	4.99	-2.61
FB08	7.88	5.08	-2.80
FB09	8.32	5.20	-3.12
FB10	9.25	4.97	-4.28
FB11	7.35	5.12	-2.23
FB12	9.45	5.25	-4.20
FB13	7.89	5.15	-2.74
FB14	8.87	5.39	-3.48

Table 3-5. Yield Stress of Test Solutions

Test	Initial Yield Stress (Pa)	Final Yield Stress (Pa)	Change in Yield Stress (Pa)
FB01	21.4	4.1	-17.3
FB02	22.0	3.2	-18.8
FB03	20.8	3.9	-16.9
FB04	14.2	3.6	-10.6
FB05	16.6	3.5	-13.1
FB06	17.4	3.5	-13.9
FB07	13.5	3.0	-10.5
FB08	13.6	3.1	-10.5
FB09	13.6	3.1	-10.5
FB10	21.2	4.1	-17.1
FB11	14.1	3.1	-11.0
FB12	21.1	3.8	-17.3
FB13	13.3	3.1	-10.2
FB14	18.5	3.6	-14.9

Lastly, the yield stress of each test solution was measured. The yield stress showed the most variability of all measured properties, ranging from 13 to 22 Pa. The test solutions containing the higher contribution of simulated AN-102 Sr/TRU precipitate yielded the lower yield stresses at the start of testing. After 30 days of testing, all solutions measured similar and much lower values (3 - 4 Pa).

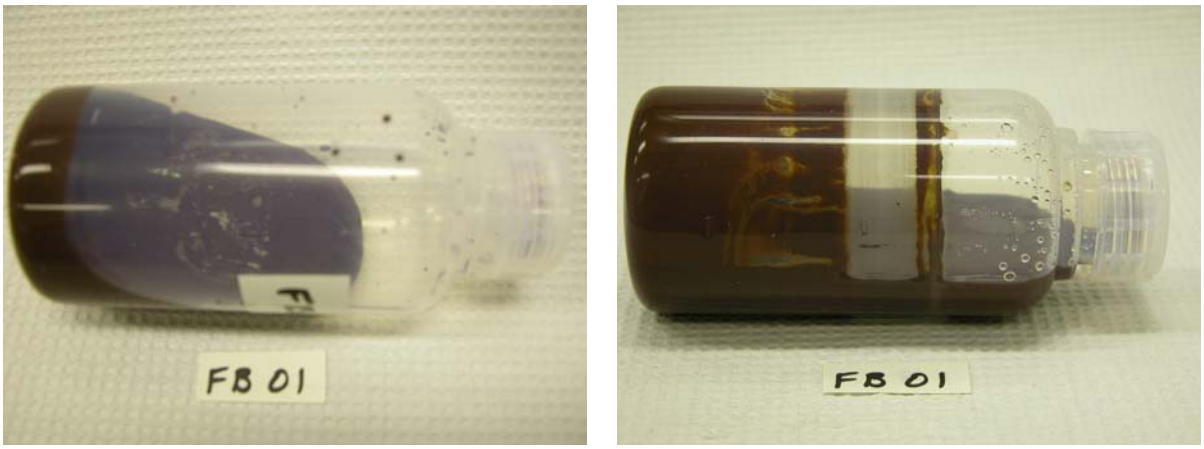

Figure 3-2. Photographs of Test FB-01 at the start of testing and after 30 days

Figure 3-3. Photographs of Test FB-14 at the start of testing and after 30 days

3.2.2 Chemical Analysis

Chemical analysis of both liquid and solid phases of all of the test solutions was performed at the conclusion of testing (see Appendix G). X-ray diffraction (see Appendix H) and scanning electron microscopy were performed on the solutions insoluble solids as well. Table 3-6 shows the measured and predicted sodium concentrations for the test solution supernate. The sodium concentration varied from 0.19 to 0.70 M and was dominated largely by the contribution of cesium eluate concentrate. The measured and predicted values show excellent agreement. The measured nitrate concentration is also shown in Table 3-6. Table 3-6 emphasizes the effect of cesium eluate on supernate chemistry (specifically sodium and nitrate) within each of the three groups of three tests at the three ratios of sludge to precipitate. The variation observed in the sodium and nitrate concentrations within the High, Middle, and Low groups is due to the varying contribution of AN-102 precipitate. With the exception of sodium and nitrate, most analytes in solution have similar concentrations.

Similar to the supernate, the solids from each test appear remarkably similar except for two main species: chromium and manganese. Table 3-7 shows that the main species (aluminum, iron, cadmium, and zirconium) remain essentially constant throughout the 14 tests. As expected, the concentration of strontium and manganese vary substantially due to the varying contribution of simulated AN-107 precipitate. Scanning electron microscopy of the solids from the 14 tests shows little variation with iron, aluminum, zirconium, cadmium and silicon present in about the same ratios. Strontium and manganese are detected only in those mixtures with the largest contribution of AN-107 precipitate. X-ray diffraction (see Appendix H) showed mixtures of aluminum, silicon, and sodium oxides (similar to that of the simulated AZ-102 sludge). Tests FB-04, 07, 08, 09, 11, 13, and 14 all showed the presence of strontium carbonate as well. Tests FB-07, 08, 09, 11, and 13 all contained the highest levels of simulated AN-102 Sr/TRU precipitate, while Tests FB-04 and 14 contained an intermediate level of precipitate.

Table 3-6. Effect of Cesium Eluate on Sodium and Nitrate Concentrations in Test Solution Supernate

Test	Sodium (M)		Nitrate (M)	Cs Eluate
	Measured	Theoretical	Measured	Contribution*
FB-01	0.313	0.315	0.229	High
FB-02	0.192	0.208	0.112	Low
FB-03	0.253	0.261	0.176	Middle
FB-04	0.461	0.481	0.261	High
FB-05	0.356	0.377	0.177	Low
FB-06	0.415	0.429	0.224	Middle
FB-07	0.696	0.648	0.361	High
FB-08	0.557	0.547	0.224	Low
FB-09	0.600	0.597	0.266	Middle
FB-10	0.249	0.261	0.176	Middle
FB-11	0.587	0.596	0.266	Middle
FB-12	0.248	0.261	0.189	Middle
FB-13	0.600	0.597	0.265	Middle
FB-14	0.418	0.429	0.226	Middle

*The cesium eluate contribution has been simplified to three levels of contribution to the tests to emphasize its effect on supernate composition.

Table 3-7. Effect of AN-102 Precipitate on Strontium and Manganese Concentrations in Test Solution Solids

Test	Al ug/g	Fe ug/g	Cd ug/g	Zr ug/g	Sr ug/g	Mn ug/g	AN-102 Precipitate Contribution*
FB-01	111000	232000	33900	33200	70	8350	None
FB-02	115000	243000	35000	32200	50	8080	None
FB-03	116000	249000	37200	34200	50	8320	None
FB-04	118000	259000	37300	34900	9090	12720	Middle
FB-05	124000	250000	36300	33700	9720	13910	Middle
FB-06	118000	232000	34300	31600	9540	13020	Middle
FB-07	121000	243000	35200	33000	20610	17880	High
FB-08	119000	242000	35100	32700	20450	17890	High
FB-09	116000	245000	35500	34200	20100	17520	High
FB-10	128000	262000	37900	33700	110	12260	None
FB-11	116000	234000	34400	31900	19250	17110	High
FB-12	120000	247000	36100	32900	70	9350	None
FB-13	120000	233000	34100	31300	19220	20620	High
FB-14	123000	248000	35900	31700	10050	14610	Middle

*The contribution of AN-102 precipitate has been simplified to reflect the three levels of addition to emphasize its effect on strontium and manganese.

3.2.3 Statistical Analysis

A statistical review of the test results from this study is provided in this section. The analyses presented were conducted using JMP Version 5.0 [8]. The statistical design used for this testing is provided in Table 2-4 (see Appendix A for more information). One of the important responses for these experimental trials was weight percent (wt %) solids. Table 3-3 provides this value for each of the 14 experimental trials.

Exhibit 1 in Appendix I provides plots of the wt % solids values versus the factor levels and groupings of the experimental trials. The four groupings of these experiments, which are plotted in this exhibit, are in support of the checks for reproducibility and for an off-spec resin effect. Group 0 is a catch-all grouping with groups 1 through 3 being of primary interest. These later 3 groups show good reproducibility among the trials in each group and show no indication of an off-spec resin effect. (In the Appendix, an open circle is used to represent the two trials with off-spec resin present.)

Several models were explored to best define the relationships between wt % solids and the factors of this study. Exhibit 2 in Appendix I provides the results of fitting the wt % solids to linear mixture model [9] of the volume fractions (vfs) of simulated AZ-102 sludge (referred to in Appendix A and I as HLW lag sludge), simulated AN-102 Sr/TRU precipitate (referred to in Appendix A and I as HLW lag TRU), and simulated AN-102 cesium eluate concentrate (referred to in Appendix A and I as Cs Conc). This model accounts for over 95% of the variation seen in the wt % solids values and is expressed as

$$\text{wt\% solids} = 15.3009 \cdot \text{HLW lag sludge} + 8.4142 \cdot \text{HLW lag TRU} + 2.1899\,\text{Cs conc}$$

where the HLW lag sludge, HLW lag TRU, and Cs conc are expressed as volume fractions and the sum of their values equals 1. Even though significant, the coefficients do not match the solids concentrations as might have been expected. A lack of fit test is included as part of the results in Exhibit 2. The repeated trials are used to estimate the pure error of the experimentation; the modeling error is compared to this pure error to test for a lack of fit for the model. The results provided in the exhibit show that there is no indication of a lack of fit for the model.

3.3 RESULTS FROM MATHEMATICAL MODELING

Experimental results were assessed against numerical predictions of solution mixture behavior made with the most recent version of the *Environmental Simulation Program* available from OLI Systems, Inc. (Morris Plains, New Jersey). Results of physical properties data are contained in Table 3-8 through Table 3-12. Two different modeling outputs are provided: 36 mL Case and pH 11.7 Case. These differ in how the preparation of simulated AZ-102 sludge was modeled. In the 36 mL Case, the required volume of concentrated sodium hydroxide added to the acidic solution was limited to 36 mL. In the pH 11.7 Case, the endpoint pH after addition of concentrated sodium hydroxide was set at pH 11.7 (rather than prescribing the quantity of sodium hydroxide added). The latter more closely resembles actual sludge makeup, however, the former more closely mimics the volume of sodium hydroxide added. Herein lies one of the first concerns with using OLI ESP in this situation: OLI ESP is not designed to perform solution pH modeling tasks with much accuracy.

Examination of the wt % solids data in Table 3-8 shows that the difference between the two OLI ESP cases is about 2 - 3 wt % solids. The 36 mL Case initially comes close to matching the measured solids concentration. However, the latter tests showed deviation from the measured values. The pH 11.7 Case showed the same bias, but with greater solids concentration in the first tests. Based upon the data, the 36 mL Case offers the best fit. In both the density and solution pH determinations (Table 3-9 and Table 3-10), the two OLI ESP cases matched each other extremely well. Both cases differed significantly in magnitude from the measured values. However, values for individual tests within the data sets showed the same relative trends. Viscosity predictions between the two cases (see Table 3-11) are also in agreement. It was not possible to compare the predicted and measured viscosities since OLI RSP predicts only the supernate viscosity (in the absence of solids). Lastly, Table 3-12 provides the OLI ESP Enthalpy of Mixing data for the two cases. The values are relatively small and reflect the small change in temperature observed in the actual tests.

Table 3-8. Comparison of Measured vs. OLI ESP Predicted Solids Concentration

Test	Wt % Solids		
	Measured	36 mL Case	pH 11.7 Case
FB-01	14.83	14.18	17.72
FB-02	15.10	14.49	18.09
FB-03	14.94	14.34	17.92
FB-04	14.61	15.67	18.89
FB-05	14.78	16.01	19.27
FB-06	14.61	15.85	19.09
FB-07	14.10	16.87	19.74
FB-08	14.33	17.29	20.20
FB-09	14.33	17.08	19.98

Table 3-9. Comparison of Measured vs. OLI ESP Predicted Density

Test	Density (g/mL)		
	Measured	36 mL Case	pH 11.7 Case
FB-01	1.140	1.041	1.043
FB-02	1.139	1.036	1.037
FB-03	1.149	1.038	1.040
FB-04	1.156	1.053	1.055
FB-05	1.147	1.048	1.050
FB-06	1.146	1.050	1.052
FB-07	1.160	1.074	1.075
FB-08	1.143	1.068	1.069
FB-09	1.130	1.071	1.072

Table 3-10 Comparison of Measured vs. OLI ESP Predicted Solution pH

Test	Solution pH		
	Measured	36 mL Case	pH 11.7 Case
FB-01	10.90	13.40	13.49
FB-02	11.05	13.40	13.49
FB-03	11.03	13.40	13.49
FB-04	11.38	13.47	13.52
FB-05	11.46	13.47	13.52
FB-06	11.45	13.47	13.52
FB-07	11.67	13.42	13.46
FB-08	11.73	13.41	13.45
FB-09	11.71	13.42	13.45

Table 3-11. OLI ESP Predicted Supernate Viscosity

Test	Viscosity (cP)	
	36 mL Case	pH 11.7 Case
FB-01	1.05	1.07
FB-02	1.04	1.06
FB-03	1.04	1.06
FB-04	1.05	1.06
FB-05	1.04	1.06
FB-06	1.04	1.06
FB-07	1.07	1.08
FB-08	1.06	1.07
FB-09	1.06	1.07

Table 3-12. OLI ESP Predicted Enthalpy of Mixing

Test	Enthalpy of Mixing(cal/g Slurry)	
	36 mL Case	pH 11.7 Case
FB-01	-0.305	-0.288
FB-02	-0.159	-0.147
FB-03	-0.233	-0.219
FB-04	-0.983	-0.829
FB-05	-0.878	-0.733
FB-06	-0.926	-0.780
FB-07	-0.814	-0.880
FB-08	-0.668	-0.744
FB-09	-0.742	-0.811

4.0 DISCUSSION

4.1 EMPIRICAL RHEOLOGY

The shear stress, σ is the force that a flowing fluid exerts on a surface. Equivalently, it is the momentum transferred to the fluid by a moving surface [Reference 10]. If the fluid flows between two surfaces a distance h apart at a velocity υ, then the shear rate is $\gamma\cdot = \upsilon/h$. The shear rate required to move a slurry at velocity υ in turbulent flow through a pipe with diameter d is $\dot{\gamma} = 8\upsilon/d$ [Reference 11].

The *shear* (or *dynamic*) viscosity is $\eta = \sigma/\dot{\gamma}$. *Liquid-like* fluids begin deforming at this viscosity immediately, as shown by Figure 4-1: they do not have an elastic (viscoelastic) regime. *Solid-like* fluids, on the other hand, store some of the energy from applied forces internally. And they can return the energy when the forces are released. These fluids typically have more complex microstructures and offer one or more mechanisms to accommodate energy input. The result is that in order to actually flow, some minimum amount of energy must be imparted to initiate mechanisms which lead to permanent, relative movement of the material. This minimum is represented by the stress level, σ_y, the *yield stress*. The simplest response to additional energy input is continuous flow under constant shearing at the stress level σ_y, as shown by Figure 4-1. Other responses, however, are possible, such as hardening or softening (σ increases or decreases with increasing strain).

Complex fluids can respond to deformation energy with a variety of different mechanisms and these can come into play at various shearing rates. But the simplest solid-like fluids have an essentially singular response and flow at the same shear stress (σ_y) at any shear rate. This is shown by Figure 4-2. This means that the viscosity decreases with increasing shear rate, $\eta \propto \dot{\gamma}^{-1}$, as shown by Figure 4-3. This is known as *shear thinning*. Liquid-like fluids, on the other hand, do not exhibit shear thinning. Instead, as shown by Figure 4-3, they have a constant viscosity, and the shear stress increases with increasing shear rate, $\sigma \propto \dot{\gamma}$, as shown by Figure 4-2. Liquid-like fluids are also called *Newtonian*.

Complex fluids arise because their constituents interact with each other by molecular forces and adapt configurations to minimize the associated free energy. Application of forces to these fluids alters the configurations, or *microstructures*, and alterations occur which eventually minimize the free energy again; whether the time scale is adequate to support this quest is, however, another matter. The molecular forces leading to microstructure formation are few: excluded volume (repulsive, leads to orientational ordering), van der Waals, and electrostatic are the primary ones, but hydrogen bonding, hydrophobic, and various solvation forces can also be important in some fluids [10]. High-level waste consists of very tiny (as small as nanometers) solid particles that accrete, or agglomerate into larger configurations in solution.

Figure 4-4 shows how various types of solid particles could interact to produce various microstructures in Hanford waste materials [11].

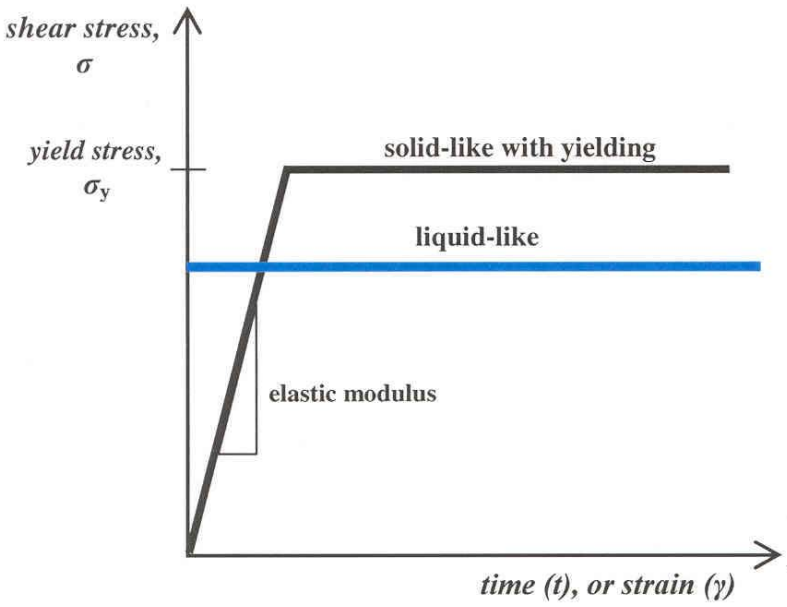

After Larson (1999). A simple liquid flows immediately under an applied stress; as long as flow continues the stress level need not change. Simple liquids do not store deformation energy; they have no elastic response. Even simple solids have an elastic response to an imposed stress: these stresses are (ideally) reversible and proportional to the strain (Hooke's law); they arise from forces of attraction between the particles comprising the solid. When the stress level reaches the yield stress σ_y, irreversible, *plastic* deformation begins and, since the solid is "simple," continues at the same stress level. The particles comprising the solid suffer relative translations and acquire new neighbors.

Figure 4-1. Shear Stress Levels During Shearing for Simple Solid and Liquid Materials

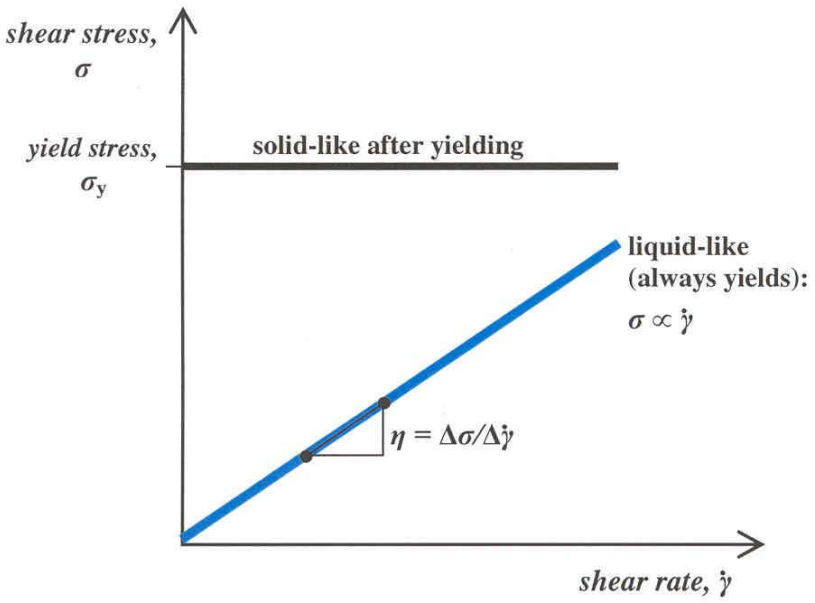

After Larson (1999). Simple liquids flow however small the applied stress is. And the larger the shear stress is, the faster is the shear rate. The viscosity, η, is defined as the ratio of small increments in stress and strain rate: $\eta = \Delta\sigma/\Delta\dot{\gamma}$. For simple liquids this is a constant (independent of shear strain and shear rate, time, stress, *etc.*), and therefore there is a simple relationship between the shear stress and shear rate, $\sigma = \eta\ \dot{\gamma}$, in which the viscosity plays an analogous role to Young's modulus in elasticity. The simplest solid-like fluids behave even simpler, always flowing under the same stress σ, regardless of the shear rate: $\sigma = \sigma_y$.

Figure 4-2. Shear Stresses versus Shear Rates for Simple Solid and Liquid Materials

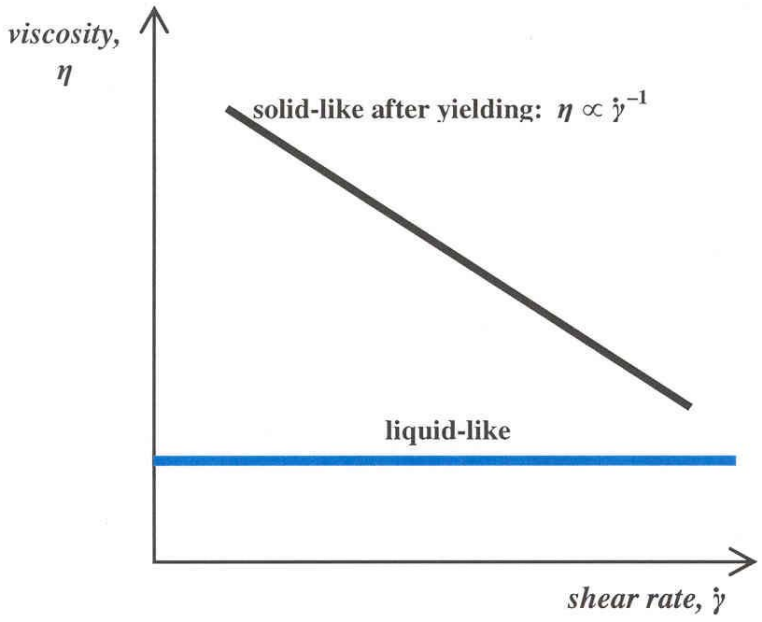

After Larson (1999). As discussed in the prior figure, simple liquids have constant viscosities, they are *Newtonian*. Simple solid-like liquids, on the other hand, have viscosities which decrease in direct proportion to the shear rate: *i.e.*, they are *shear-thinning*.

Figure 4-3. Viscosity versus Shear Rates for Simple Solid and Liquid Materials

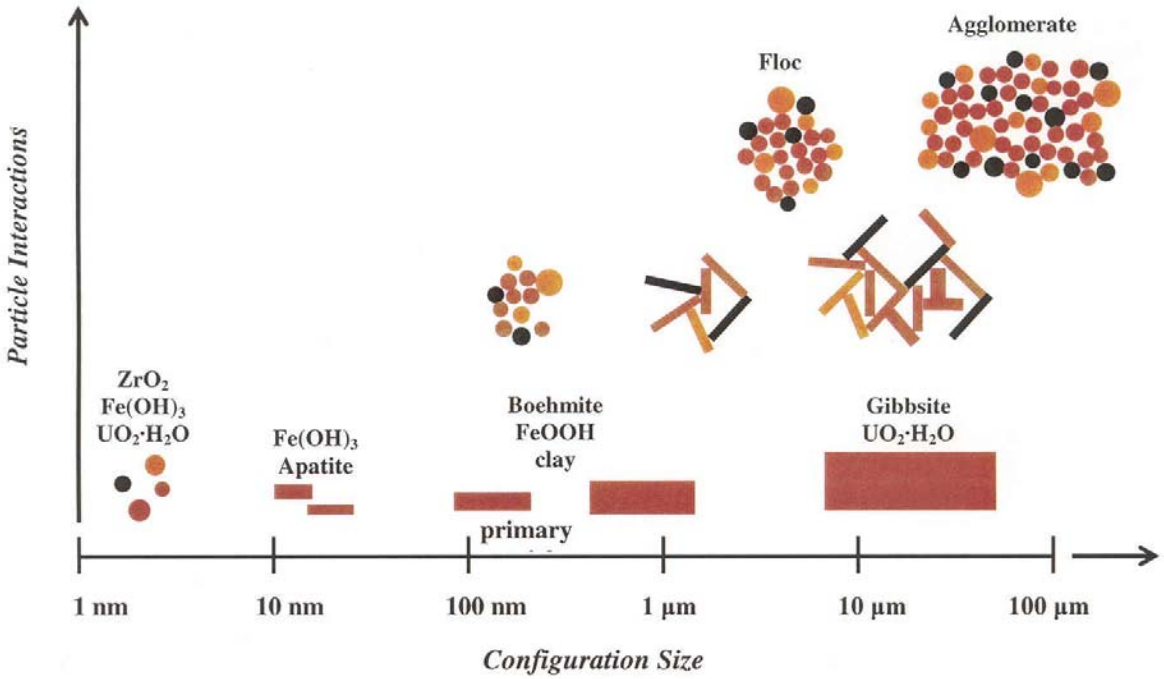

The smallest particles in Hanford waste are oxides and hydrous oxides such as ZrO_2 and FeOOH having diameters in the 3 to 6 nm range. Larger particles like boehmite (AlOOH) and apatite ($Ca_5[PO_4]_3[OH,F,Cl]$) have sizes ranging from 0.1 to 1 µm. These submicron "primary" particles form agglomerates with sizes between about 1 to 10 µm. Flocculation results in even larger configurations.

Figure 4-4. Particles and Associated Configurations for Hanford Waste Materials

(Reference: Jewett 2002)

Particle agglomeration bears on the slurry transport properties (e.g., viscosity and shear strength) which determine mixing performance for gas retention and release (i.e., hydrogen) and waste homogenization (i.e., slurry settling). Although small, dense, primary particles in the waste may approach theoretical mineral densities, agglomerates may have very much reduced effective densities. Such effective densities are used to determine and characterize the slurry transport properties. It turns out that the volume fraction of primary particles, V_P, within an agglomerate can be expressed as [11]

Equation 4-1 $$V_P = (R/r)^{D-3}$$

where
R = average agglomerate size,
r = average primary particle size,
D = scale factor.

For example, $D \approx 2$ for a boehmite agglomerate, and with $R \approx 1.5$ μm and $r \approx 0.05$ μm, the fraction that boehmite mineral particles occupy within an agglomerate of boehmite is $V_P \approx 0.04$. So these particles only occupy about 4% of the agglomerate volume.

The effective density of the agglomerated particles in a slurry is equal to the volume-weighted average density of the mineral (dry-basis solids) and the interstitial liquid. Jewett [11] reports the dry solids densities (ρ_{solids}) for HLW in 8 Hanford tanks. This information is provided in Table 4-1. It can be used to relate the centrifuged sludge liquid and solid densities, ρ_{CL} and ρ_{SL}, respectively, to the bulk density of the sludge, ρ_B, and the bulk density of the sludge before it is centrifuged, ρ_C:

Equation 4-2 $\rho_C = x\{(1 - n)\,\rho_{CS} + n\,\rho_{CL}\} + (1 - x)$, **for centrifuged sludge**

Equation 4-3 $C_V = x(1 - n)$, **for actual (in-tank) sludge**

Equation 4-4 $\rho_B = C_V\,\rho_S + (1 - C_V)\,\rho_L$, **for actual (in-tank) sludge**

Equation 4-5 $y = C_V\,\rho_S/\rho_B$ **or** $1 - y = (1 - C_V)\,\rho_L/\rho_B$, **for actual (in-tank) sludge**

These terms have the following meanings:

C_V	solid volume fraction of actual (in-tank) sludge
n	porosity of the solid layer after the sludge is centrifuged and standing liquid is decanted
x	volume fraction of the resulting solid layer after the sludge is centrifuged and standing liquid decanted
y	weight fraction of the solids within the sludge
ρ_B	bulk density of the sludge
ρ_C	bulk density of the sludge before it is centrifuged
ρ_{CS}	solid density of the sludge after it is centrifuged and standing liquid is decanted
ρ_{CL}	liquid density of the sludge after the sludge is centrifuged
ρ_S	density of solids in the sludge

Measurements of the terms in Equation 4-1 through Equation 4-5 from actual Hanford waste are provided in Table 4-2. Additional information is provided in Table 4-3**.**

Table 4-1. Major Constituents in the Dry-Basis Compositions of Hanford HLW

Compound	Hanford Tank Waste							
	AW-103	**AY-101**	**AY-102**	**AZ-101**	**AZ-102**	**C-104**	**C-107**	**SY-102**
$Al(OH)_3$	9.0	26.4	30.6	57.8	46.9	39.6	25.4	53.6
Bi_2O_3							5.9	
Cr_2O_3								9.2
FeO(OH)		27.9	37.4	26.1	33.6	7.5	17.5	7.3
$KAlSiO_4$					6.1			
$Mn(OH)_2$			8.2					
$Na_2C_2O_4$		13.7						
$Na_2U_2O_7$	11.4					12.1		
$Na_7F(PO_4)_2 \cdot 19H_2O$							30.6	19.3
$NaAlCO_3(OH)_2$		9.3	15.1					
$NaAlSiO_4$		14.9				8.5	15.2	
NaF	36.5					9.4		
ZrO_2	36.4			7.3		14.9		
Dry-Solids Density, ρ_{solids} (g/ml)	3.5	2.9	3.1	3.0	3.1	3.1	2.2	2.3

from Jewett 2002

Table 4-2. Measured Sludge Properties from 10 Hanford HLW Storage Tanks

Tank	Density, g/ml					Weight Fraction of Solid, y	Solid Volume Fraction C_V	Volume Reduction from Centrifuge x
	Bulk, ρ_B	Liquid, ρ_L	Centrifuged Liquid, ρ_{CL}	Solid, ρ_S	Centrifuged Solid, ρ_C			
AZ-101	1.67 1.62	1.2 1.2	1.22 1.22		1.67 1.62			0.71 0.76
AZ-102	1.49	1.1	1.13		1.49			0.64
SY-102	1.56	1.03				0.605		
AY-101	1.59	1.0	1.14				0.657	
AY-102	1.4 1.4	1.0 0.99				0.456		
AW-103	1.43	1.00	1.0		1.75			0.97
AW-104	1.44	0.988						
C-104	1.46 – 1.97	1.10						
C-106	1.17	1.55		2.28				
C-107	1.17	1.44					0.662	

from Jewett 2002

Table 4-3. Estimated Sludge Properties from 10 Hanford HLW Storage Tanks

Tank	Density, g/ml		Solid Volume in Sludge, C_V (vol.%)	Porosity in Sludge	Fully Mixed Solid Volume (vol.%)
	Liquid, ρ_L	Solid, ρ_S			
AZ-101	1.20	2.19	45.0	0.550	2.5
AZ-102	1.10	1.97	45	0.55	4.7
SY-102	1.25	2.24	32.5	0.675	3.7
AY-101	1.00	1.90	65.7	0.343	38.8
AY-102	0.99	2.68	23.8	0.762	6.90
AW-103	1.00	1.96	45.0	0.550	12.1
AW-104	0.988	1.99	45.0	0.550	34.2
C-104	1.10	3.11	29.6	0.704	N/A: SST
C-106	1.17	2.28	34.2	0.658	N/A: SST
C-107	1.17	1.44	66.2	0.338	N/A: SST

from Jewett 2002

Laboratory results are often reported as grams of dry solids per liter of slurry, say C. The volume fraction C_V, is therefore

Equation 4-6 $$C_V = 0.001C/\rho_{solids}$$

where ρ_{solids} is the particle density given in the last row of Table 4-1

The viscosity of a slurry η can be expressed in a number of different ways. After, Jewett [11], we will treat the slurry as a mixture of solid and liquid phases and assign a separate value to the liquid phase, η_L, and a value η_M for the solids-liquid mixture comprising the slurry. For a slurry with low solids (< 1 vol.%) in laminar flow,

Equation 4-7 $$\eta_M = \eta_L(1 + 2.5C_V)$$

Jewett [11] recommends a general modification to this relationship allows extension to higher particle volume fractions, and inclusion of the shear rate:

Equation 4-8 $$\eta_M = \eta_L\left[1 + aC_V + bC_V^2 + c\{\exp(dC_V) - 1\}\right]\dot{\gamma}^n$$

Here, a, b, c, d, and n are adjustable parameters, and n must be a negative number to represent shear thinning materials; the equation can also be used without subtracting 1 from the exponential term. Jewett's analysis of Hanford tank data provides the following correlations from Equation 4-8:

Equation 4-9 $$\eta_M = 2.0\left[1 + 2.5C_V + 10.05C_V^2 + 1.3\{\exp(17C_V) - 1\}\right]\dot{\gamma}^{-0.06} \text{ cP} \quad \text{(nominal)}$$

Equation 4-10 $$\eta_M = 1.6\left[1 + 2.5C_V + 10.05C_V^2 + 21\exp(39C_V)\right]\dot{\gamma}^{-0.75} \text{ cP} \quad \text{(upper bound)}$$

This analysis is based on an assumed particle density of 3 g/mL, used to convert from laboratory-supplied solids concentration in g/L to volume percent solids.

Table 4-4 shows data from the Hanford Tank Farms which illustrates the effects of temperature and solids content on viscosity, η_M. As expected, it shows that η_M increases with an increasing amount of solids in the waste, and that it decreases with increasing temperature. Introductory material from which these trends can be understood is provided in the next section.

Table 4-4. Viscosity Measurements for Three High-Level Waste Feed Tanks

Tank	Viscosity (cP)	Solids Content (g/L)	Temperature (ºC)	Tank	Viscosity (cP)	Solids Content (g/L)	Temperature (ºC)
AY-102	1.78	0	27	C-104	7.9	200	45
	1.12	0	45		31.2	300	45
	0.32	0	65		23.5	620	45
	2.29	75.8	27		1.5	0	65
	0.93	75.8	45		1.3	60	65
	1.06	75.8	65		1.8	100	65
	2.05	101	27		3.7	140	65
	1.19	101	45		7.3	200	65
	1.29	101	65		32.5	300	65
	3.01	151.6	27		18.9	620	65
	1.73	151.6	45	AZ-101	2.25	0	27.7
	0.89	151.6	65		2.34	0	44.9
	3.64	210	27		1.66	0	64.9
	2.66	210	45		2.28	18.4	27.6
	1.73	210	65		1.97	18.4	44.9
*~~AY-102~~	~~1.36~~	~~210~~	~~27~~		2.26	18.4	64.9
C-104	1.7	0	27		2.95	36.8	27.3
	2.6	60	27		2.09	36.8	45.1
	3.2	100	27		2.19	36.8	64.7
	5.5	140	27		3.23	155	27.4
	8	200	27		1.90	155	45.1
	29.7	300	27		2.27	155	64.9
	43.6	620	27		7.19	301	27.4
	1.6	0	45		7.03	301	27.3
	1.5	60	45		4.41	301	44.9
	2.4	100	45		5.63	301	44.9
	4.6	140	45		2.91	301	64.7

*Data seems out of place.

4.2 RELATIONSHIP BETWEEN MICROSTRUCTURAL FEATURES AND RHEOLOGICAL PROPERTIES

The rheology of liquids and liquid-like solids are controlled by constituents of the liquid such as particles and the interactions of the constituents. Suspensions of small particles, or "colloids" in a liquid phase provide a much different rheology than liquids with "gelled" colloidal suspensions; in the latter case the particles interact and clump together [10]. While thermodynamics drives clumping of the components dispersed in a liquid, flow can sometimes enhance this. Spheroidal particles larger than about a micron tend to settle out unless the particle density matches that of the liquid so that the force of gravity is balanced; but if the liquid is very viscous, settling can be effectively inhibited. Particles are kept in the suspended state by Brownian motion, a process that also produces the particle collisions which can lead to aggregation. The ratio of gravitational to Brownian forces must exceed one to avoid sedimentation,

Equation 4-11 $$a^4 \Delta\rho g / k_B T > 1$$

where a is the average particle radius, $\Delta\rho$ the density difference $\rho_{solid} - \rho_{liquid}$, g = 980 cm/s is the gravitational constant, and $k_B T$ is the Boltzmann constant × temperature; the Brownian stress is

Equation 4-12 $$\sigma_{Brown.} = k_B T / a^3$$

Particles larger than about a micron tend to settle when $\Delta\rho \sim 1$ g/cm3. "Flow-induced migration" and "particle-inertia" effects can also produce inhomogeneous distributions of larger particles.

Even suspensions of non-interacting, undeformable spheres can produce complex rheology [10]. Flow fields around one particle can, for example, affect those around neighboring particles. So as particle concentrations (C_V) increase, Equation 4-7 eventually fails. Also, at high C_V, the viscosity becomes sensitive to particle properties such as surface roughness, size, and shape factors (e.g., the particle size distribution). For example, when particles having very different particle sizes are mixed, the viscosity can be much lower than when the particle volume fraction is achieved with monosized particles.

While a simple liquid can have a constant viscosity, more complex fluids have viscosities which depend on other factors, the simplest of which is the shear-rate. A shear-rate dependency such as shear thinning arises when the shear-rate is high enough to disturb the distribution of interparticle spacings from their equilibrium values. The rate of return to equilibrium for the particles is controlled by the particle diffusivity, D_0, which is just

Equation 4-13 $$D_0 = k_B T/(6\pi\eta_L a)$$

for dilute solutions. The time required for a particle to diffuse a distance equal to its radius is

Equation 4-14 $$t_D = a^2/D_0 = 6\pi\eta_L a/k_B T$$

And this is related to a shear-rate effect by the Peclet number, Pe, which is proportional to the product of the shear-rate and t_D, $\mathrm{Pe} \propto \dot{\gamma} t_D$:

Equation 4-15 $$\mathrm{Pe} \equiv \eta_L \dot{\gamma} a^3/k_B T$$

For particle concentrations above some value but less than an upper bound (such as the maximum packing fraction ϕ_m, which is about 0.63 for spheres) suspensions can produce an "apparent yield stress" σ_y below which there is no flow and above which the viscosity decreases towards a limiting value say η_∞. The viscosity can be expressed as

Equation 4-16 $$\eta_M = \eta_\infty + (\eta_0 - \eta_\infty)/(1 + \sigma/\sigma_C)$$

where $\sigma_C \equiv k_B T/a^3 b$ is the critical shear stress required for shear thinning, with b denoting an adjustable parameter, and η_0 is the *zero-shear viscosity*. The zero-shear viscosity can be estimated by the product of the "characteristic shear modulus," G, and the "characteristic relaxation time, τ:

Equation 4-17 $$\eta_0 \sim G\tau$$

So a viscous fluid with viscosity η_0 can be viewed as a "relaxing solid" with shear modulus (ratio of shear stress to shear strain, $G \equiv \sigma/\gamma$) that relaxes in time τ.

The "flow curves" for fluids exhibiting a yield stress are often fit by the constitutive relation for a *Bingham plastic*:

Equation 4-18 $$\sigma = \sigma_y + \eta_{pl}\dot{\gamma}$$

where η_{pl} is the "plastic viscosity," which is the viscosity the mixture exhibits under this type of flow. Larson [10] claims that better representation is, however, obtained with the Casson equation:

Equation 4-19 $$\sigma^{1/2} = \sigma_y^{1/2} + C\dot{\gamma}^{1/2}$$

As the volume fraction increases particle interactions can result in the deformation of pliable particles [10]. For volume fractions less than about 0.4 suspensions of soft spheres have viscosities similar to those of hard spheres. But at higher levels differences develop and, instead of Equation 4-16, better results could be obtained by fitting the data with

Equation 4-20 $$\eta_M = \eta_\infty + (\eta_0 - \eta_\infty)/(1 + [\sigma/\sigma_C]^m)$$

where m is an adjustable parameter larger than one.

The hydrodynamic component takes up most of the load at high shear stresses, making the Brownian contribution ($\sigma_{Brown.} = k_B T/a^3$) insignificant [10]. This provides for the formation of strings of particles parallel to the flow direction. These strings can become ordered into hexagonal arrays in the plane perpendicular to the flow direction. With increasing shear stresses, the shear thinning regime can be replaced with shear thickening. Even hard particles should exhibit some shear thickening at high shear stresses, but this behavior is probably promoted by softer particles.

Suspensions of hard spheres also produce liquids with some elasticity because Brownian movement tends to restore distorted particles to their original conditions [10]. This process also leads to the development of normal stresses. The Brownian contribution to the fluid elasticity is a "low frequency" effect: $\nu_{low} \sim D_s/a^2$, where D_s is the "short-time" diffusivity, which is a function of C_V. Nearby particles develop lubrication forces while undergoing relative motion and are therefore slow to approach their initial configuration. At "high frequencies" on the other hand, particles are forced to move through the solvent much faster than they can relax by a diffusive process, and this regime is characterized by a constant, high-frequency viscosity, η'_∞.

This parameter is a function of C_V through the short-time diffusivity:

Equation 4-21 $$\eta'_\infty(C_V) = k_B T/[6\pi D_s(C_V)a] = \eta_L D_0/D_s(C_V)$$

using Equation 4-14 for the second expression. The "high-frequency" is $\nu_{high} \sim k_B T/(\eta'_\infty a^3)$. As C_V increases, D_s decreases and η'_∞ increases because as particles move over one another the solvent is forced through increasingly smaller interparticle gaps.

Elongated particles tend to "bulk up" liquids [10]. Viscosity increases with increasing concentration of such particles as does the tendency to display shear thinning. Much lower volume fractions of elongated particles are required to produce strong rheological effects than spherical particles. This is because diluteness requires that the rods or plates be able to rotate freely without interacting with neighbors. As the aspect ratio (*length/diameter*) increases so does the zero-shear viscosity, and the tendencies to display shear thinning and elasticity. The volume fraction of rods is given by

Equation 4-22 $$C_V = \pi d^2 L N_V/4$$

where d and L are the diameter and length of the rods and N_V is the number of them per unit volume. *Dilute* solutions have $N_V < 1/L^3$; *semi-dilute* $1/L^3 < N_V < 1/dL^2$; and *concentrated* solutions have $N_V > 1/dL^2$. The ratio of viscous to Brownian stresses decreases as $(N_V L^3)^{-2}$ as the concentration increases in the semi-dilute regime. The rheology of solutions containing elongated particles is affected by geometrical effects such as rod-jamming and ordering; liquid crystal formation (nematic phase) is an example of the latter.

Gelation, of flocculation occurs when an agent (*p*H modifier, electrolyte, or polymer) is added to the solution which reduces the particle-particle repulsive forces and thereby allows the ubiquitous van der Waals forces of attraction to be unopposed until shorter interparticle spacings and multi-particle structures are obtained [10]. If particle concentrations are high enough, a sample-spanning network results. Let X denote the interparticle spacing and W the effective potential energy of the particle-particle interactions; W is the sum of repulsive terms (e.g., "crowding" or *steric*) and attractive terms (e.g., van der Waals, electrostatic, and hydration). The potential energy has a minimum value, $W_{min.}$, which defines the equilibrium (zero stress/strain) interparticle spacing. The properties of the floc depend strongly on $W_{min.}$, which is a negative number (to represent attraction). For example, the viscosity of a gel increases exponentially with the magnitude $|W_{min.}|$ of attraction:

Equation 4-23 $$\eta_0 \propto \exp(-\alpha W_{min}/k_B T)$$

where α is a constant ($-\alpha W_{min} > 0$). This is a consequence of the increased relaxation time particles require to change their positions:

Equation 4-24 $$\tau \approx (a^2/D_0)\exp(-\alpha W_{min}/k_B T)$$

The larger $W_{min.}/k_BT$ is and the more strongly a gel is flocculated, the longer it takes to reach thermodynamic equilibrium, and the low shear-rate viscosity η_0 increases too. Furthermore, the drop in viscosity in the shear thinning region becomes steeper: Figure 4-5 shows a sudden decrease in viscosity above a critical shear stress, the yield stress σ_y. In a strongly flocculated media once particle-particle contacts are formed they are released so infrequently by thermal agitation that particle rearrangements are strongly suppressed. The time for the structure to equilibrate following deformation is too long to be observed: the "Newtonian" zero shear viscosity is only attained at $\dot{\gamma} < \tau^{-1}$, which are lower than those measured in the experiment. Thus, strongly flocculating gels are characterized by yield stress not the zero-shear viscosity.

The mechanical properties of a gel depend on particle dimensions and concentration as well as flocculation strength (i.e., $W_{min.}$) [10]. The shear modulus, G, for such gels is strain-dependent and can, for example, exhibit effects such as strain softening. Weakly flocculated gels are less strain sensitive than strongly flocculated gels. As the strength of the floc increases so does its tendency to display brittle behavior.

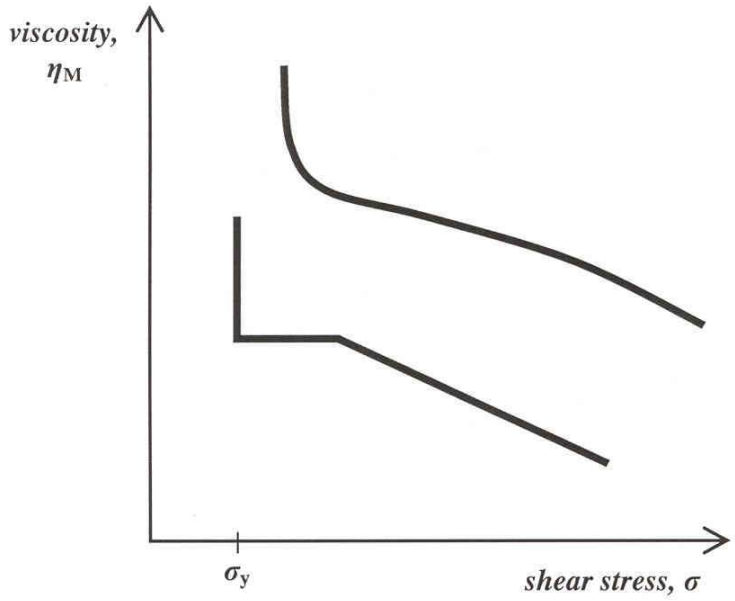

After Larson (1999). More complex fluids exhibit sudden decreases in viscosity above a critical shear stress called the *yield stress*, σ_y. The top curve represents the behavior more like that from a real material. Thus, defining the yield stress accurately can be experimentally challenging.

Figure 4-5. Viscosity versus Shear Stress for More Complex Fluids

Some mechanical properties can be obtained by considering a static, as opposed to thermodynamic equilibrium. Consider a pair of particles being pulled apart by a strain γ. Their separation increases by γr_0, where $r_0 = 2a + X_0$ is the separation between the particle centers without strain. Then the strain increases the gap between the particle surfaces from X_0 to

Equation 4-25 $$X = X_0 + \gamma(2a + X_0)$$

A force $F = -dW/dX$ is produced by this increased separation. The macroscopic shear stress is this force multiplied by the number of interparticle bonds per unit area, which scales as $(C_V/a)^2$:

Equation 4-26 $$\sigma \approx F(C_V/a)^2$$

The yield strain occurs at the minimum of $W(X)$ versus X, which occurs when $d^2W/dX^2 = 0$, and represents the separation X_y which tears the particles apart. A crude estimate of the yield stress is

Equation 4-27 $$\sigma_y \sim (C_V/a)^2 F(X_y)$$

where $F(X_y) \sim W_{min.}/X_0$. Since $[d^2W/dX^2](X_0) \approx [dW/dX](X)/(X - X_0) \approx F(X)/2\gamma a$,

Equation 4-28 $$F(X) \approx 2\gamma a[d^2W/dX^2](X_0)$$

and $G \equiv \sigma/\gamma \approx [F(C_V/a)^2]/\gamma$ can be estimated as

Equation 4-29 $$G \sim [2C_V^2/a][d^2W/dX^2](X_0)$$

Equation 4-29 states that the shear modulus is controlled by the curvature of the particle-particle potential W at the minimum, $W_{min.}$.

Gel networks break down and subsequently reform at high shear rates [10]. The steady-state shear stress may become linearly dependent on the shear rate in this regime, Extrapolation of this linear relationship back to zero shear rate intersects the stress axis at a positive value, σ_B, called the *Bingham* yield stress:

Equation 4-30 $$\sigma = \sigma_B + \eta_{pl}\dot{\gamma}$$

The Bingham yield stress differs from the "true" yield stress σ_y; σ_y is measured at small shearing strains by finding the minimum stress required to induce flow.

It has been recognized for quite some time that gas retention and release from HLW is strongly influenced by the density, yield strength, and viscosity of the waste [Reference 12]. Elastic properties are currently being evaluated more intensely as also playing a significant role in this particular rheological issue. For example, Johnson et al. [Reference 13] have applied the principles of linear-elastic fracture mechanics to model gas release from ocean sediments.

This page intentionally left blank.

5.0 CONCLUSIONS AND FUTURE WORK

Assessment of the results obtained from testing did not yield any recognizable problematic solutions, properties, or conditions. The high viscosity and yield stress of the simulated sludge and the resulting test mixtures that included it are of note, however. Otherwise, the results of this task do not suggest the necessity of any additional work. Planned radioactive testing for verification purposes is slated at a later time when the materials are available.

This page intentionally left blank.

6.0 REFERENCES

1. Barnes, M.J., *Task Technical and Quality Assurance Plan for HLW Lag Storage and Feed Blending*, WSRC-TR-2002-00429, Rev. 0, Savannah River Site, Aiken, SC 29808 (2002).

2. Barnes, M.J., *Experimental Design for RPP Study on High Level Waste Lag Storage and Feed Blending*, WSRC-RP-2003-00155, Rev. 0, Savannah River Site, Aiken, SC 29808 (2003).

3. Sherwood, D.J. *Recycle Stream Blending for High and Low Level Waste*, 24590-WTP-TSP-RT-01-025, Rev. 0, Hanford Reservation, Richland, WA 99352 (2001).

4. Barnes, M.J., Sherwood, D.J., Laurinat, J.E., Edwards, T.B., Fondeur, F.F., and P.R. Burkett, *Recycle Stream Blending for High and Low Level Waste*, WSRC-TR-2003-00156, Rev. 0, Savannah River Site, Aiken, SC 29808 (2003).

5. Zamecnik, J.R., Baich, M.A., Hansen, E.K., and M.R. Poirier, *AN-102 Simulant Sr/TRU Precipitation and Ultrafiltration*, WSRC-TR-2003-00056, Rev. 0, Savannah River Site, Aiken, SC 29808 (2003).

6. Pierce, R.A. and A.S. Choi, *Cesium Eluate Evaporation Solubility and Physical Property Behavior*, WSRC-TR-2002-00411, Rev. 0, Savannah River Site, Aiken, SC 29808 (2002).

7. Hansen, E.K., Eibling, R.E., and T.B. Calloway, Jr., *Mixing Envelope D Sludge with LAW Intermediate Products with and without Glass Formers,* WSRC-TR-2001-00203, Rev. 0, Savannah River Site, Aiken SC 29808 (2001).

8. SAS Institute, Inc., *JMP® Statistics and Graphics Guide*, Version 5, SAS Institute, Inc., Cary, NC, 2002.

9. Cornell, J. A., *Experiments with Mixtures: Designs, Models, and the Analysis of Mixture Data*, Third Edition, John Wiley & Sons, Inc., New York, 2002.

10 Larson, R.G., *The Structure and Rheology of Complex Fluids*, Oxford University Press, New York (1999).

11. Jewett, J.R., RPP-9805, *Values of Particle Size, Particle Density, and Slurry Viscosity to Use in Waste Feed Delivery Transfer System Analysis*, CH2M Hill Hanford Group, Inc., Richland, WA (2002).

12. Meyer, P.A., *et al.*, *Gas Retention and Release Behavior in Hanford Double-Shell Tanks*, PNNL-11536, Rev. 1, Pacific Northwest National Laboratory, May (1997).

13. Johnson, B.D., B.P Boudreau, B.S. Gardiner, and R. Maass, *Mechanical Response to Bubble Growth*, Marine Geology, vol. 187, p. 347-363 (2002).

This page intentionally left blank.

APPENDIX A.
STATISTICAL DESIGN DEVELOPMENT

In general the approach used for this design effort is as follows: the two input streams are considered as a mixture (see Cornell [1]). The set of design points is generated using a combination of extreme vertices for the mixture region and selected levels of other factors of interest in this study. The details of this approach are presented in the sections that follow.

Defining the Factor Levels
Two streams/tanks are of primary interest in this blending study: high-level waste (HLW) lag storage washed solids and cesium (Cs) concentrate. Upper and lower bounds for the streams/tanks are provided in Table A- 1. Upper and lower bounds on the volume fractions were selected in an attempt to bound the likely contributions from these two sources.

Table A- 1. Nominal Volume Fraction for Each Input Stream/Tank with Lower and Upper Limits

Stream/Tank	Short ID	Lower	Upper
HLW Lag Storage Washed Solids	HLW lag	0.9643	0.9818
Cs Concentrate	Cs Conc	0.0182	0.0357

The bounds of Table A- 1 define the factor space for this study. However, there is a restriction on the feasible values of these two factors: only the relative volumes of these two inputs being blended are of interest. Mathematically, the restriction on the blend of these two factors may be stated as in Equation 0-1.

Equation 0-1. $$\text{HLW lag} + \text{Cs conc} = 1$$

where each term in this equation represents the volume fraction of the indicated stream in the blend or mixture, and, as indicated, the sum of these volume fractions must equal one.

In addition to supporting the investigation of these two primary factors, additional requirements that this design must meet include:

- The design contains two experiments that include an additional stream in the feed blend: the off-specification resin stream. This additional stream is to make up 0.35 volume percent (or 0.0035 volume fraction) of the feed blend for each of these two experiments. The purpose of introducing these spiked trials into the test matrix is to provide a gross check for effects on the properties of the feed blend due to this additional input stream.
- For this study, the HLW lag stream is to consist of sludge with and without TRU precipitate. Three ratios of sludge to TRU (sludge:TRU) are to be covered in the test matrix; these are 90:10, 90:5, and 100:0. The purpose of introducing these variations in the HLW lag composition is to allow for an assessment of the sensitivity of the models relating feed properties to blends of the three primary factors of this study to these variations.

Selecting the Model Form

Statistical methods for the design and analysis of mixture experiments are available (see Cornell [9]). Software is also available (see Reference [8]) to assist with these problems, and the use of this software is facilitated by the selection of candidate models that are to be explored in relating each response of interest (e.g., a physical property of the resulting blend such as viscosity) to the components of the mixture. The restrictions imposed by Equation 0-1 have an impact on the candidate models. Specially, there is no intercept term in a model involving a mixture. Thus, the model for a response variable, y, expressed as a linear function of the mixture components (HLW lag and Cs conc) would be of the form:

Equation 0-2. $$y = \alpha_1 \cdot (\text{HLW lag}) + \alpha_2 \cdot (\text{Cs conc}) + \varepsilon$$

where ε represents an error term for the model and α represents unknown coefficients, which may or may not be of practical significance. These coefficients are estimated from the data generated by the designed experiment.

While Equation 0-2 does provide an opportunity for exploring possible linear effects between the mixture components and a response of interest, more complex relationships between the components and the response require more complex models such as the mixture response surface model given in equation (3).

Equation 0-3. $$y = \beta_1 \cdot (\text{HLW lag}) + \beta_2 \cdot (\text{Cs conc}) + \beta_3 \cdot (\text{HLW lag}) \cdot (\text{Cs conc}) + \varepsilon$$

where ε represents an error term for the model and β represents unknown coefficients, which may or may not be of practical significance. Once, again, the coefficients are estimated from the data generated by the designed experiment.

Selecting a Test Matrix

Criteria have been developed for use in selecting an optimal test matrix from a set of candidate design points for a mixture experiment, and software [8] is available to facilitate the use of these criteria. However, the simplicity of this two-component mixture problem allows for the development of a test matrix without having to appeal to such software.

It is a very straightforward process to determine the two extreme vertices of the mixture space defined by the upper and lower limits of Table A- 1. Averaging these two pairs of points provides the centroid of the mixture region. These three points, which are provided in Table A- 2, provide the data needed to fit the model given by Equation 0-3.

Table A- 2. Extreme Vertices (EVs) and Centroid for Mixture Space Defined by the Values of Table A- 1 in Volume Fractions

Type	HLW Lag	Cs Conc
EV	0.96430	0.03570
EV	0.98180	0.01820
Centroid	0.97305	0.02695

These 3 design points selected for the test matrix do not distinguish among the variations of interest for HLW lag. These variations need to be brought into the test matrix. To accomplish this, each row of Table A- 2 is included three times in the final test matrix – once for each of the possible ratios of sludge to TRU.

The two trials spiked with the off-specification resin stream that are needed in the test matrix are to be introduced as variations of the centroid blend of the two primary streams. For one variation, the HLW lag is to consist of only sludge while the other variation is to be 90% sludge and 10% TRU.

To provide a check on the reproducibility of the test results, the centroid given in Table A- 2 is added to the final test matrix three times – once for each of the possible ratios of sludge to TRU. This completes the experiments making up the final test matrix, which is provided in Table 3. Trial (or experimental) identifiers (IDs) are provided in this table as well.

Table A- 3. Final Test Matrix for this Study

Description	Trial ID	HLW lag (vf)	HLW Lag sludge (vf)	HLW Lag TRU (vf)	Cs Conc (vf)	Off-Spec Resin (vf)
HLW lag is sludge only.	FB01	0.96430	0.96430	0.00000	0.03570	0.00000
	FB02	0.98180	0.98180	0.00000	0.01820	0.00000
	FB03	0.97305	0.97305	0.00000	0.02695	0.00000
HLW lag: 95% sludge and 5% TRU	FB04	0.96430	0.91609	0.04822	0.03570	0.00000
	FB05	0.98180	0.93271	0.04909	0.01820	0.00000
	FB06	0.97305	0.92440	0.04865	0.02695	0.00000
HLW lag: 90% sludge and 10% TRU	FB07	0.96430	0.86787	0.09643	0.03570	0.00000
	FB08	0.98180	0.88362	0.09818	0.01820	0.00000
	FB09	0.97305	0.87575	0.09731	0.02695	0.00000
Runs spiked with off-spec resin stream	FB10	0.96955	0.96955	0.00000	0.02695	0.00350
	FB11	0.96955	0.87260	0.09696	0.02695	0.00350
Duplicate runs for reproducibility	FB12	0.97305	0.97305	0.00000	0.02695	0.00000
	FB13	0.97305	0.87575	0.09731	0.02695	0.00000
	FB14	0.97305	0.92440	0.04865	0.02695	0.00000

(vf – volume fraction)

The duplicate centroid design points provide an opportunity for assessing the repeatability of the testing (experimental and associated analytical) process, both within and between the variations of the HLW lag stream. These data will serve as the basis for evaluating the trials "spiked" with the off-specification resin stream. The data of Table A- 3 also support the fitting of Equation 0-3 for each variation of the sludge to TRU ratio for the HLW Lag stream. Comparing these fitted equations should provide a basis for evaluating the impact of the HLW lag stream sludge to TRU ratio on the properties of the resulting feed blend.

The sequencing, placement, and analyses of these 14 experimental trials should be as random as is practical and should be recorded as part of the information associated with this part of the feed blend matrix study.

Concluding Comments

Using statistical methods associated with designing and modeling mixture experiments, a test matrix was developed in this memo for the next phase of the Feed Blending Matrix study for RPP. The data generated from this design should provide an opportunity to investigate for significant (both statistical and practical) effects over the associated, experimental factor space of interest.

APPENDIX B.
COMPOSITION OF STOCK FEED SOLUTIONS

Supernate Analysis

Analyte	Method	Units	Simulated AZ-102 Sludge	Simulated AN-102 PPT	Simulated Cs Eluate	IX Resin
sodium	ICP-ES	Molar	0.0961	3.55	6.22	0.003
potassium	ICP-ES	Molar	0.0000352	0.0208	0.0307	0.0000910
total OH	Titration	Molar	0.0655	1.08	0.002	< 0.0020
free OH	Titration	Molar	< 0.010	0.448	< 0.0020	< 0.0020
carbonate	Titration	Molar	0.0181	0.344	< 0.0020	< 0.0020
nitrate	IC	Molar	0.0112	0.977	6.27	< 0.0016
nitrite	IC	Molar	0.0264	0.522	< 0.0022	< 0.0022
formate	IC	Molar	< 0.00011	0.00913	< 0.0022	< 0.0022
fluoride	IC	Molar	0.00895	0.0395	< 0.0011	< 0.0011
chloride	IC	Molar	0.00677	0.0465	< 0.0006	< 0.0006
phosphate	IC	Molar	0.00015794	0.0124	< 0.0011	< 0.0011
sulfate	IC	Molar	0.00239	0.0467	0.0180	< 0.0005
oxalate	IC	Molar	0.00011364	0.0182	< 0.0011	< 0.0011
Ag	ICP-ES	mg/L	< 0.30	< 0.60	8.25	< 0.60
Al	ICP-ES	mg/L	0.274	4050	7.64	0.480
B	ICP-ES	mg/L	21.5	125	88.7	73.0
Ba	ICP-ES	mg/L	< 0.012	< 0.024	4.33	< 0.024
Ca	ICP-ES	mg/L	0.529	59.2	261	4.06
Cd	ICP-ES	mg/L	< 0.014	17.7	< 0.028	< 0.028
Ce	ICP-ES	mg/L	< 0.77	< 1.54	< 1.54	< 1.54
Co	ICP-ES	mg/L	< 0.044	< 0.088	0.518	< 0.088
Cr	ICP-ES	mg/L	5.71	1.87	142	< 0.10
Cu	ICP-ES	mg/L	< 0.050	2.59	15.5	< 0.10
Fe	ICP-ES	mg/L	< 0.044	< 0.088	10.9	< 0.088
La	ICP-ES	mg/L	< 0.70	<1.4	< 1.4	< 1.4
Li	ICP-ES	mg/L	< 0.10	< 0.20	< 0.20	< 0.20
Mg	ICP-ES	mg/L	0.12	< 0.17	8.26	1.49
Mn	ICP-ES	mg/L	< 0.0090	1.41	3.01	0.0369
Mo	ICP-ES	mg/L	0.599	16.8	< 0.20	< 0.20
Nb	ICP-ES	mg/L	< 0.50	< 1.0	< 1.0	< 1.0
Nd	ICP-ES	mg/L	< 0.26	< 0.52	< 0.52	< 0.52
Ni	ICP-ES	mg/L	< 0.062	121	0.694	< 0.12
P	ICP-ES	mg/L	0.741	375	1.49	< 1.36
Pb	ICP-ES	mg/L	< 0.69	29.2	< 1.4	< 1.4
Re	ICP-ES	mg/L	< 0.050	< 0.10	< 0.10	< 0.10
S	ICP-ES	mg/L	64.5	1510	671	5.03
Si	ICP-ES	mg/L	7.81	4.34	3.28	1.80
Sn	ICP-ES	mg/L	< 0.26	< 0.52	< 0.52	< 0.52
Sr	ICP-ES	mg/L	0.156	5.55	8.81	0.0186
Ti	ICP-ES	mg/L	< 0.14	< 0.28	< 0.28	< 0.28
V	ICP-ES	mg/L	0.163	< 0.26	1.04	0.311
Zn	ICP-ES	mg/L	< 0.37	< 0.74	< 0.74	< 0.74
Zr	ICP-ES	mg/L	< 0.048	0.343	< 0.096	< 0.096

Solids Analysis

Analyte	Method	Units	Simulated AZ-102 Sludge	Simulated AN-102 PPT	Simulated Cs Eluate	IX Resin
Ag	ICP-ES	µg/g	570	< 310	NA*	< 310
Al	ICP-ES	µg/g	136200	8720	NA	< 245
B	ICP-ES	µg/g	780	5030	NA	3850
Ba	ICP-ES	µg/g	790	1610	NA	< 13
Ca	ICP-ES	µg/g	2610	8690	NA	770
Cd	ICP-ES	µg/g	40800	90	NA	< 15
Ce	ICP-ES	µg/g	1620	1060	NA	< 785
Co	ICP-ES	µg/g	720	< 45	NA	< 45
Cr	ICP-ES	µg/g	2380	770	NA	< 51
Cu	ICP-ES	µg/g	280	430	NA	< 51
Fe	ICP-ES	µg/g	279000	2340	NA	61
K	ICP-ES	µg/g	1830	2160	NA	1690
La	ICP-ES	µg/g	8750	830	NA	< 715
Li	ICP-ES	µg/g	< 97	< 105	NA	< 105
Mg	ICP-ES	µg/g	2250	570	NA	200
Mn	ICP-ES	µg/g	9990	98300	NA	100
Mo	ICP-ES	µg/g	< 97	< 105	NA	< 105
Na	ICP-ES	µg/g	NA	125000	NA	2190
Nb	ICP-ES	µg/g	< 484	< 510	NA	< 510
Nd	ICP-ES	µg/g	361	1610	NA	< 265
Ni	ICP-ES	µg/g	NA	1880	NA	< 65
P	ICP-ES	µg/g	3220	6630	NA	< 695
Pb	ICP-ES	µg/g	3560	3740	NA	< 705
Re	ICP-ES	µg/g	< 49	< 51	NA	< 51
S	ICP-ES	µg/g	< 484	2250	NA	< 510
Si	ICP-ES	µg/g	10000	2090	NA	2550
Sn	ICP-ES	µg/g	< 252	< 265	NA	< 265
Sr	ICP-ES	µg/g	45	231000	NA	2.03
Ti	ICP-ES	µg/g	660	< 145	NA	< 145
V	ICP-ES	µg/g	< 126	< 135	NA	< 135
Zn	ICP-ES	µg/g	5010	< 380	NA	< 380
Zr	ICP-ES	µg/g	34700	< 50	NA	120

*NA = insufficient solids were present to obtain an analysis.

APPENDIX C.
RHEOLOGY OF STOCK FEED SOLUTIONS

Rheometer:		Haake RS600
Geometry:		Concentric Cylinder Z41
Measuring Temperature:		25°C
Ramp Program	Up	0 - 1000 sec^{-1}, 5 minutes
	Hold	1000 sec^{-1}, 1 minute
	Down	1000 - 0 sec^{-1}, 5 minutes
Data fitted	Samples	Down Curve
	NIST Standard	Up and Down
Range fitted	Samples	100 - 1000 sec^{-1}
	NIST Standard	0 - 1000 sec^{-1}

All sludges were non-Newtonian and fitted as a Bingham Plastic

	Average	Average	Yield (Pa)		Consistency (cP)		R^2		
	Yield (Pa)	Consistency (cP)	1st	2nd	1st	2nd	1st	2nd	Notes:
15 wt % AZ-102	0.6	4.85	0.6	0.6	4.86	4.84	0.9942	0.9955	Taylor Vortices
AN-102 Cesium Eluate	0.0	3.05	0.0	0.0	3.06	3.05	0.9986	0.9990	Newtonian, Taylor Vortices
Spent Resin Supernate	0.0	0.93	0.0	0.0	0.93	0.93	0.9970	0.9971	Newtonian, used cone/plate

S3 NIST traceable viscosity standard, Lot # F102609, viscosity = 3.266 cP at 25°C

	Viscosity (cP)	R^2
3 STD_R1	3.36	0.9997

All sludges were non-Newtonian and fitted as a Bingham Plastic

	Average	Average	Yield (Pa)		Consistency (cP)		R^2		
	Yield (Pa)	Consistency (cP)	1st	2nd	1st	2nd	1st	2nd	Notes:
14.7 wt % AZ-102 Sludge	19.9	7.92	20.1	19.8	7.97	7.86	0.9930	0.9918	Thixotropic, Slip

N35 NIST traceable viscosity standard, Lot # F102205, viscosity = 50.49 cP at 25°C

	Viscosity (cP)	R^2
N35 STD_R1	51.91	0.9998

This page intentionally left blank.

APPENDIX D.
X-RAY DIFRACTIONS OF STOCK FEED SOLUTIONS

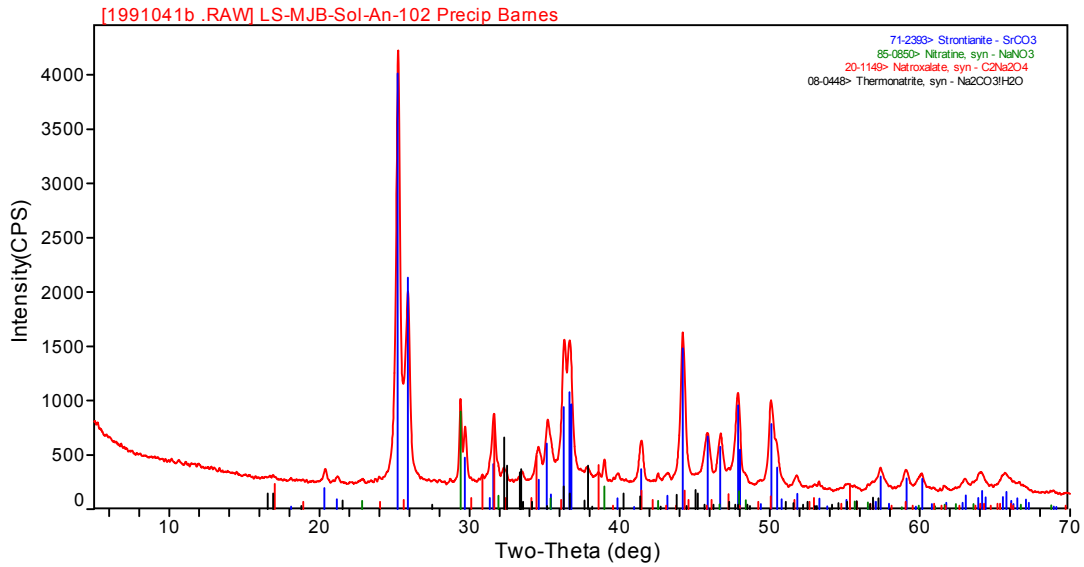

Figure D- 1. Simulated AN-102 Sr/TRU Precipitate

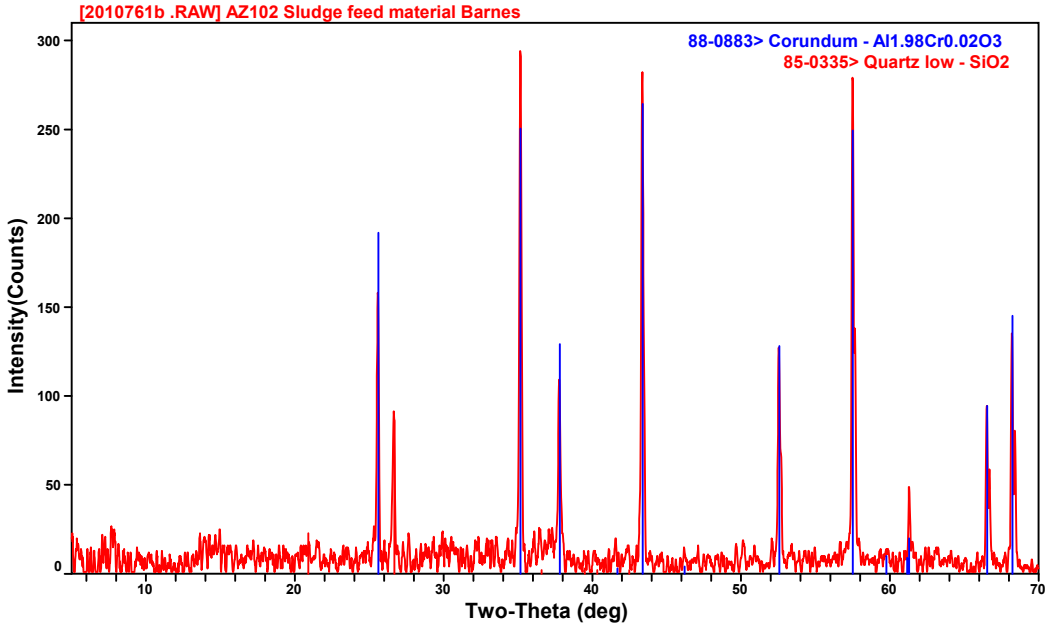

Figure D- 2. Simulated AZ-102 Sludge

This page intentionally left blank.

APPENDIX E.
AZ-102 SLUDGE SIMULANT PREPARATION

The following recipe is used to prepare 1L of sludge (unconcentrated).

1. Place 500 g of water in a 2-L beaker.
2. Dissolve 0.66 g of potassium permanganate ($KMnO_4$) in the water.
3. Add 2.24 g of 50 wt % manganous nitrate solution ($Mn(NO_3)_2$-$4H_2O$) and mix.
4. Add the following to the mixture while stirring.

Compounds	Formula	Mass (g)
Ferric Nitrate	$Fe(NO_3)_3.9H_2O$	511.305
Nickel Nitrate	$Ni(NO_3)_2.6H_2O$	25.706
Zirconyl nitrate	$ZrO(NO_3)_2.xH_2O$ x~6	38.921
Cerium nitrate	$Ce(NO_3)_3.6H_2O$	1.539
Lanthanum nitrate	$La(NO_3)_3.6H_2O$	7.087
Neodymium Nitrate	$Nd(NO_3)_3.6H_2O$	0.227
Barium Nitrate	$Ba(NO_3)_2$	0.576
Calcium Nitrate	$Ca(NO_3)_2.4H_2O$	1.901
Cadmium Nitrate	$Cd(NO_3)_2.4H_2O$	28.249
Chromium Nitrate	$Cr(NO_3)_3.9H_2O$	3.901
Cobalt Nitrate	$Co(NO_3)_2.6H_2O$	0.187
Copper Nitrate	$Cu(NO_3)_2.3H_2O$	0.006
Magnesium Nitrate	$Mg(NO_3)_2.6H_2O$	6.592
Lead Nitrate	$Pb(NO_3)_2$	0.032
Strontium Nitrate	$Sr(NO_3)_2$	0.003
Zinc Nitrate	$Zn(NO_3)_2.6H_2O$	1.343
Silver Nitrate	$AgNO_3$	0.234

5. Measure the pH (value obtained was 1.0).
6. Add enough 8 M NaOH to bring the pH above 10 (actual pH value was 11.7 after 1 hour of stirring).
7. Add 400 mL of 0.6 M Na_2CO_3 and mix well.
8. Measure the pH (pH was 11.8).
9. Allow slurry to settle and decant. (Actual volumes obtained: 930 mL settled sludge, 350 mL decanted filtrate).

10. Wash the slurry with equal volume of wash solution (0.01 M NaOH and 0.01 M $NaNO_2$), allow it to settle and decant (sludge volume remained about the same as at the start).
11. Repeat the equal volume wash & decant step six more times to get the nitrate level below 1000 mg/L.
12. The final volume after the last wash& decant was 1000 mL.
13. Add 0.026 g of insoluble titanium dioxide (TiO_2), 1.623 g of silica (SiO_2), and 21.596 g of aluminum oxide (Al_2O_3) and mix thoroughly.
14. Add the following and stir to dissolve.

Compounds	**Formula**	**Mass Needed**
Boric Acid	H3BO3	0.418
Sodium Chloride	NaCl	0.687
Sodium Fluoride	NaF	0.212
Sodium Sulfate	Na2SO4	0.569
Sodium Phosphate	Na3PO4.12H2O	11.012
Sodium Nitrite	NaNO2	0.841

15. The resulting slurry was measured and found to be 7.2 wt % solids. It was further concentrated with a crossflow filter apparatus to 14.8 wt %.

APPENDIX F.
RHEOLOGY OF INDIVIDUAL TESTS

Initial Test Measurements

Rheometer:		Haake RS600
Geometry:		Concentric Cylinder Z41
Measuring Temperature:		25°C
Ramp Program	Up	0 - 1000 sec^{-1}, 5 minutes
	Hold	1000 sec^{-1}, 1 minute
	Down	1000 - 0 sec^{-1}, 5 minutes
Data fitted	Samples	Down Curve
	NIST Standard	Up and Down
Range fitted	Samples	100 - 1000 sec^{-1}
	NIST Standard	0 - 1000 sec^{-1}

All sludges were non-Newtonian and fitted as a Bingham Plastic

	Average	Average	Yield (Pa)		Consistency (cP)		R^2		
	Yield (Pa)	Consistency (cP)	1st	2nd	1st	2nd	1st	2nd	Notes:
FB-01	21.4	9.69	20.3	22.5	9.73	9.64	0.9986	0.9959	Thixotropic, Slip
FB-02	22.0	9.31	22.0	22.0	9.37	9.24	0.9975	0.9978	Thixotropic, Slip
FB-03	20.8	9.55	19.7	21.9	9.55	9.55	0.9979	0.9981	Thixotropic, Slip
FB-04	14.2	7.60	13.1	15.2	7.09	8.11	0.9973	0.9982	Thixotropic, Slip
FB-05	16.6	8.67	16.5	16.8	8.33	9.01	0.9983	0.9988	Thixotropic, Slip
FB-06	17.4	8.80	17.5	17.4	8.71	8.89	0.9986	0.9981	Thixotropic, Slip
FB-07	13.5	7.60	13.5	13.4	7.88	7.32	0.9976	0.9931	Slightly Thixotropic
FB-08	13.6	7.88	13.6	13.7	7.88	7.88	0.9982	0.9981	Thixotropic
FB-09	13.6	8.32	13.4	13.8	8.29	8.36	0.9995	0.9992	Thixotropic
FB-10	21.2	9.25	21.0	21.5	9.36	9.14	0.9900	0.9336	Thixotropic, Slip
FB-11	14.1	7.35	13.2	15.0	7.86	6.83	0.9952	0.8685	Thixotropic
FB-12	21.1	9.45	19.9	22.3	9.28	9.62	0.9993	0.9979	Thixotropic, Slip
FB-13	13.3	7.89	13.1	13.4	7.83	7.96	0.9984	0.9980	Thixotropic, Slip
FB-14	18.5	8.87	18.3	18.6	8.87	8.88	0.9979	0.9979	Thixotropic, Slip

N35 NIST traceable viscosity standard,
Lot # F102205, viscosity = 50.49 cP at 25°C

	Viscosity (cP)	R^2
N35 STD_R1	51.96	0.9998
N35 STD_R2	51.82	0.9998

Post-Test Results

Rheometer:		Haake RS600
Geometry:		Concentric Cylinder Z41
Measuring Temperature:		25°C
Ramp Program	Up	0 - 1000 sec^{-1}, 5 minutes
	Hold	1000 sec^{-1}, 1 minute
	Down	1000 - 0 sec^{-1}, 5 minutes
Data fitted	Samples	Down Curve
	NIST Standard	Up and Down
Range fitted	Samples	100 - 1000 sec^{-1}
	NIST Standard	0 - 1000 sec^{-1}

All sludges were non-Newtonian and fitted as a Bingham Plastic

	Average	Average	Yield (Pa)		Consistency (cP)		R^2	
	Yield (Pa)	Consistency (cP)	1st	2nd	1st	2nd	1st	2nd
FB-01-2	4.1	5.34	4.1	4.2	5.33	5.36	0.9927	0.9932
FB-02-2	3.2	5.27	3.3	3.2	5.27	5.27	0.9916	0.9936
FB-03-2	3.9	5.22	3.9	3.9	5.22	5.22	0.9950	0.9919
FB-04-2	3.6	5.25	3.6	3.7	5.23	5.28	0.9925	0.9942
FB-05-2	3.5	5.15	3.4	3.6	5.06	5.24	0.9926	0.9959
FB-06-2	3.5	5.16	3.5	3.6	5.15	5.17	0.9940	0.9943
FB-07-2	3.0	4.99	3.0	3.1	5.00	4.99	0.9959	0.9910
FB-08-2	3.1	5.08	3.1	3.0	4.98	5.19	0.9947	0.9962
FB-09-2	3.1	5.20	3.1	3.1	5.21	5.19	0.9953	0.9957
FB-10-2	4.1	4.97	4.4	3.9	4.62	5.33	0.9488	0.9875
FB-11-2	3.1	5.12	2.9	3.2	5.11	5.13	0.9933	0.9922
FB-12-2	3.8	5.25	3.6	3.9	5.17	5.33	0.9929	0.9950
FB-13-2	3.1	5.15	3.1	3.1	5.13	5.18	0.9954	0.9942
FB-14-2	3.6	5.39	3.5	3.6	5.35	5.43	0.9948	0.9947

N35 NIST traceable viscosity standard,
Lot # F102205, viscosity = 50.49 cP at 25°C

	Viscosity (cP)	R^2
N35 STD_R1	52.24	0.9997
N35 STD_R2	51.79	0.9998

APPENDIX G.
COMPOSITION OF TEST SLURRIES

Supernate Analysis

Analyte	Method	Units	FB-01	FB-02	FB-03	FB-04	FB-05	FB-06
sodium	ICP-ES	Molar	0.313	0.192	0.253	0.461	0.356	0.415
potassium	ICP-ES	Molar	0.0010	0.0004	0.0007	0.0018	0.0013	0.0016
total OH	Titration	Molar	0.0114	0.0149	0.0180	0.0394	0.0505	0.0472
free OH	Titration	Molar	< 0.002	< 0.002	< 0.002	< 0.002	< 0.002	0.013
carbonate	Titration	Molar	0.0072	0.0097	0.0088	0.0336	0.0365	0.0310
nitrate	IC	Molar	0.229	0.112	0.176	0.261	0.177	0.224
nitrite	IC	Molar	0.0130	0.0135	0.0132	0.0374	0.0402	0.0407
formate	IC	Molar	< 0.002	< 0.002	< 0.002	0.005	0.005	0.005
fluoride	IC	Molar	0.0034	0.0036	0.0038	0.0058	0.0062	0.0063
chloride	IC	Molar	0.0033	0.0034	0.0033	0.0051	0.0055	0.0055
phosphate	IC	Molar	< 0.001	< 0.001	< 0.001	< 0.001	< 0.001	< 0.001
sulfate	IC	Molar	0.0019	0.0016	0.0017	0.0038	0.0037	0.0039
oxalate	IC	Molar	< 0.001	< 0.001	< 0.001	0.0024	0.0025	0.0026
Ag	ICP-ES	mg/L	< 0.6	< 0.6	< 0.6	< 0.6	< 0.6	< 0.6
Al	ICP-ES	mg/L	< 0.48	< 0.48	< 0.48	2.46	2.38	2.74
B	ICP-ES	mg/L	31.3	31.3	29.0	32.0	32.0	30.3
Ba	ICP-ES	mg/L	< 0.024	< 0.024	< 0.024	< 0.024	< 0.024	< 0.024
Ca	ICP-ES	mg/L	13.4	5.89	6.01	6.63	5.74	6.48
Cd	ICP-ES	mg/L	< 0.028	< 0.028	< 0.028	3.17	3.62	3.69
Ce	ICP-ES	mg/L	< 1.54	< 1.54	< 1.54	< 1.54	< 1.54	< 1.54
Co	ICP-ES	mg/L	< 0.088	< 0.088	< 0.088	< 0.088	< 0.088	< 0.088
Cr	ICP-ES	mg/L	4.27	4.25	4.33	34.6	28.7	34.4
Cu	ICP-ES	mg/L	0.10	< 0.1	< 0.1	< 0.1	< 0.1	< 0.1
Fe	ICP-ES	mg/L	< 0.088	< 0.088	< 0.088	< 0.088	< 0.088	< 0.088
La	ICP-ES	mg/L	< 1.4	< 1.4	< 1.4	< 1.4	< 1.4	< 1.4
Li	ICP-ES	mg/L	< 0.2	< 0.2	< 0.2	< 0.2	< 0.2	< 0.2
Mg	ICP-ES	mg/L	3.13	1.37	1.41	1.03	1.00	1.10
Mn	ICP-ES	mg/L	< 0.018	< 0.018	< 0.018	< 0.018	< 0.018	< 0.018
Mo	ICP-ES	mg/L	0.53	0.47	0.54	1.39	1.39	1.43
Nb	ICP-ES	mg/L	< 1	< 1	< 1	< 1	< 1	< 1
Nd	ICP-ES	mg/L	< 0.52	< 0.52	< 0.52	< 0.52	< 0.52	< 0.52
Ni	ICP-ES	mg/L	< 0.124	< 0.124	< 0.124	6.55	7.01	7.16
P	ICP-ES	mg/L	< 1.36	< 1.36	< 1.36	1.95	2.51	2.16
Pb	ICP-ES	mg/L	< 1.38	< 1.38	< 1.38	< 1.38	< 1.38	< 1.38
Re	ICP-ES	mg/L	< 0.1	< 0.1	< 0.1	< 0.1	< 0.1	< 0.1
S	ICP-ES	mg/L	72.4	60.4	64.4	142	137	146
Si	ICP-ES	mg/L	5.82	11.7	8.67	11.7	12.1	13.6
Sn	ICP-ES	mg/L	< 0.52	< 0.52	< 0.52	< 0.52	< 0.52	< 0.52
Sr	ICP-ES	mg/L	0.05	0.03	0.03	0.15	0.13	0.14
Ti	ICP-ES	mg/L	< 0.28	< 0.28	< 0.28	< 0.28	< 0.28	< 0.28
V	ICP-ES	mg/L	0.74	0.37	0.50	< 0.26	< 0.26	0.72
Zn	ICP-ES	mg/L	< 0.74	< 0.74	< 0.74	< 0.74	< 0.74	< 0.74
Zr	ICP-ES	mg/L	< 0.096	< 0.096	< 0.096	0.222	< 0.096	< 0.096

Supernate Analysis – continued

Analyte	Method	Units	FB-07	FB-08	FB-09	FB-10	FB-11	FB-12
sodium	ICP-ES	Molar	0.696	0.557	0.600	0.249	0.587	0.248
potassium	ICP-ES	Molar	0.0030	0.0023	0.0026	0.0007	0.0026	0.0007
total OH	Titration	Molar	0.1200	0.0766	0.0784	0.0225	0.0722	0.0159
free OH	Titration	Molar	0.00937	0.0122	0.00787	0.00772	0.0118	< 0.002
carbonate	Titration	Molar	0.0473	0.0525	0.0451	0.0041	0.0412	0.0087
nitrate	IC	Molar	0.361	0.224	0.266	0.176	0.266	0.189
nitrite	IC	Molar	0.0678	0.0683	0.0657	0.0132	0.0641	0.0134
formate	IC	Molar	0.012	0.011	0.011	< 0.002	0.012	< 0.002
fluoride	IC	Molar	0.0086	0.0087	0.0084	0.0038	0.0083	0.0039
chloride	IC	Molar	0.0076	0.0078	0.0074	0.0034	0.0073	0.0034
phosphate	IC	Molar	< 0.001	< 0.001	< 0.001	< 0.001	< 0.001	< 0.001
sulfate	IC	Molar	0.0069	0.0063	0.0062	0.0017	0.0061	0.0017
oxalate	IC	Molar	0.0060	0.0055	0.0054	< 0.001	0.0056	< 0.001
Ag	ICP-ES	mg/L	0.72	< 0.6	0.61	< 0.6	0.61	< 0.6
Al	ICP-ES	mg/L	24.0	25.4	24.8	< 0.48	19.4	< 0.48
B	ICP-ES	mg/L	32.0	32.2	31.0	21.1	28.5	21.3
Ba	ICP-ES	mg/L	< 0.024	< 0.024	< 0.024	< 0.024	< 0.024	< 0.024
Ca	ICP-ES	mg/L	6.20	6.10	7.17	7.10	5.85	5.74
Cd	ICP-ES	mg/L	10.07	10.45	10.22	< 0.028	9.83	< 0.028
Ce	ICP-ES	mg/L	< 1.54	< 1.54	< 1.54	< 1.54	< 1.54	< 1.54
Co	ICP-ES	mg/L	< 0.088	< 0.088	< 0.088	< 0.088	< 0.088	< 0.088
Cr	ICP-ES	mg/L	71.0	53.8	58.9	6.77	59.1	4.31
Cu	ICP-ES	mg/L	< 0.1	< 0.1	< 0.1	< 0.1	< 0.1	< 0.1
Fe	ICP-ES	mg/L	< 0.088	< 0.088	< 0.088	< 0.088	< 0.088	< 0.088
La	ICP-ES	mg/L	< 1.4	< 1.4	< 1.4	< 1.4	< 1.4	< 1.4
Li	ICP-ES	mg/L	< 0.2	< 0.2	< 0.2	< 0.2	< 0.2	< 0.2
Mg	ICP-ES	mg/L	0.73	0.72	0.87	1.50	0.79	1.33
Mn	ICP-ES	mg/L	< 0.018	< 0.018	< 0.018	< 0.018	< 0.018	< 0.018
Mo	ICP-ES	mg/L	2.50	2.36	2.43	0.46	2.32	0.50
Nb	ICP-ES	mg/L	< 1	< 1	< 1	< 1	< 1	< 1
Nd	ICP-ES	mg/L	< 0.52	< 0.52	< 0.52	< 0.52	< 0.52	< 0.52
Ni	ICP-ES	mg/L	14.7	14.9	14.7	< 0.124	14.6	< 0.124
P	ICP-ES	mg/L	7.38	7.43	8.10	< 1.36	5.68	< 1.36
Pb	ICP-ES	mg/L	< 1.38	< 1.38	< 1.38	< 1.38	< 1.38	< 1.38
Re	ICP-ES	mg/L	< 0.1	< 0.1	< 0.1	< 0.1	< 0.1	< 0.1
S	ICP-ES	mg/L	237	224	226	63.6	223	63.7
Si	ICP-ES	mg/L	17.3	25.4	26.4	16.0	20.3	10.2
Sn	ICP-ES	mg/L	< 0.52	< 0.52	< 0.52	< 0.52	< 0.52	< 0.52
Sr	ICP-ES	mg/L	0.17	0.15	0.16	0.03	0.16	0.02
Ti	ICP-ES	mg/L	< 0.28	< 0.28	< 0.28	< 0.28	< 0.28	< 0.28
V	ICP-ES	mg/L	0.55	0.67	< 0.26	0.30	0.42	0.40
Zn	ICP-ES	mg/L	< 0.74	< 0.74	< 0.74	< 0.74	< 0.74	< 0.74
Zr	ICP-ES	mg/L	< 0.096	< 0.096	< 0.096	< 0.096	< 0.096	< 0.096

Supernate Analysis – continued

Analyte	Method	Units	FB-13	FB-14
sodium	ICP-ES	Molar	0.600	0.418
potassium	ICP-ES	Molar	0.0026	0.0016
total OH	Titration	Molar	0.0863	0.0427
free OH	Titration	Molar	0.013	0.00652
carbonate	Titration	Molar	0.0408	0.0336
nitrate	IC	Molar	0.265	0.226
nitrite	IC	Molar	0.0650	0.0404
formate	IC	Molar	0.011	0.054
fluoride	IC	Molar	0.0084	0.0063
chloride	IC	Molar	0.0074	0.0055
phosphate	IC	Molar	< 0.001	< 0.001
sulfate	IC	Molar	0.0063	0.0039
oxalate	IC	Molar	0.0057	0.0027
Ag	ICP-ES	mg/L	< 0.6	< 0.6
Al	ICP-ES	mg/L	24.0	2.44
B	ICP-ES	mg/L	28.4	25.3
Ba	ICP-ES	mg/L	< 0.024	< 0.024
Ca	ICP-ES	mg/L	6.25	6.02
Cd	ICP-ES	mg/L	9.94	3.57
Ce	ICP-ES	mg/L	< 1.54	< 1.54
Co	ICP-ES	mg/L	< 0.088	< 0.088
Cr	ICP-ES	mg/L	58.1	33.9
Cu	ICP-ES	mg/L	< 0.1	< 0.1
Fe	ICP-ES	mg/L	< 0.088	< 0.088
La	ICP-ES	mg/L	< 1.4	< 1.4
Li	ICP-ES	mg/L	< 0.2	< 0.2
Mg	ICP-ES	mg/L	0.70	0.88
Mn	ICP-ES	mg/L	< 0.018	< 0.018
Mo	ICP-ES	mg/L	2.41	1.45
Nb	ICP-ES	mg/L	< 1	< 1
Nd	ICP-ES	mg/L	< 0.52	< 0.52
Ni	ICP-ES	mg/L	14.3	7.07
P	ICP-ES	mg/L	7.42	2.28
Pb	ICP-ES	mg/L	< 1.38	< 1.38
Re	ICP-ES	mg/L	< 0.1	< 0.1
S	ICP-ES	mg/L	223	144
Si	ICP-ES	mg/L	16.2	15.5
Sn	ICP-ES	mg/L	< 0.52	< 0.52
Sr	ICP-ES	mg/L	0.16	0.14
Ti	ICP-ES	mg/L	< 0.28	< 0.28
V	ICP-ES	mg/L	0.35	0.41
Zn	ICP-ES	mg/L	< 0.74	< 0.74
Zr	ICP-ES	mg/L	< 0.096	< 0.096

Solids Analysis

Analyte	Method	Units	FB-01	FB-02	FB-03	FB-04	FB-05	FB-06
Ag	ICP-ES	µg/g	560	610	640	570	590	570
Al	ICP-ES	µg/g	111000	115000	116000	118000	124000	118000
B	ICP-ES	µg/g	1300	1000	850	850	910	750
Ba	ICP-ES	µg/g	540	730	780	800	590	700
Ca	ICP-ES	µg/g	3080	2700	2850	3420	3820	3280
Cd	ICP-ES	µg/g	33900	35000	37200	37300	36300	34300
Ce	ICP-ES	µg/g	1020	1330	1320	1350	1430	1280
Co	ICP-ES	µg/g	770	680	600	650	1080	810
Cr	ICP-ES	µg/g	2910	2490	2620	2440	2520	2480
Cu	ICP-ES	µg/g	190	140	120	280	250	370
Fe	ICP-ES	µg/g	232000	243000	249000	259000	250000	232000
K	ICP-ES	µg/g	660	1160	1440	960	2510	1470
La	ICP-ES	µg/g	7250	7550	8000	8150	8040	7490
Li	ICP-ES	µg/g	< 175	< 175	< 175	< 175	< 175	< 175
Mg	ICP-ES	µg/g	2150	2070	2200	2220	2270	2140
Mn	ICP-ES	µg/g	8350	8080	8320	12720	13910	13020
Mo	ICP-ES	µg/g	< 175	< 175	< 175	< 175	< 175	< 175
Na*	ICP-ES	µg/g	NA	NA	NA	NA	NA	NA
Nb	ICP-ES	µg/g	< 890	< 890	< 890	< 890	< 890	< 890
Nd	ICP-ES	µg/g	< 350	<320	380	< 350	510	330
Ni*	ICP-ES	µg/g	NA	NA	NA	NA	NA	NA
P	ICP-ES	µg/g	3130	2980	2820	3020	3220	3290
Pb	ICP-ES	µg/g	4280	3250	3290	4300	5430	4420
Re	ICP-ES	µg/g	< 90	< 90	< 90	< 90	< 90	< 90
S	ICP-ES	µg/g	< 75	< 75	< 75	< 75	2270	1230
Si	ICP-ES	µg/g	9400	9510	9240	9680	10100	10300
Sn	ICP-ES	µg/g	< 450	< 450	< 450	< 450	< 450	< 450
Sr	ICP-ES	µg/g	70	50	50	9090	9720	9540
Ti	ICP-ES	µg/g	500	430	430	590	670	660
V	ICP-ES	µg/g	< 230	< 230	< 230	< 230	< 230	< 230
Zn	ICP-ES	µg/g	5600	4650	4320	4720	7280	5520
Zr	ICP-ES	µg/g	33200	32200	34200	34900	33700	31600

*Sodium and nickel data were unavailable due to an interference with the digestion method.

Solids Analysis - continued

Analyte	Method	Units	FB-07	FB-08	FB-09	FB-10	FB-11	FB-12
Ag	ICP-ES	µg/g	700	670	610	640	630	740
Al	ICP-ES	µg/g	121000	119000	116000	128000	116000	120000
B	ICP-ES	µg/g	760	770	780	1190	860	910
Ba	ICP-ES	µg/g	690	710	670	330	560	600
Ca	ICP-ES	µg/g	4000	4170	3840	3740	3920	2810
Cd	ICP-ES	µg/g	35200	35100	35500	37900	34400	36100
Ce	ICP-ES	µg/g	1420	1250	1260	< 1340	< 1120	1080
Co	ICP-ES	µg/g	990	1050	950	1360	1000	890
Cr	ICP-ES	µg/g	2570	2380	2300	2990	2330	2650
Cu	ICP-ES	µg/g	260	240	220	580	240	180
Fe	ICP-ES	µg/g	243000	242000	245000	262000	234000	247000
K	ICP-ES	µg/g	2350	5250	3140	3310	3450	590
La	ICP-ES	µg/g	7770	7810	7850	8230	7380	7680
Li	ICP-ES	µg/g	< 175	< 175	< 175	< 175	< 175	< 175
Mg	ICP-ES	µg/g	2130	2180	2440	2370	2330	2150
Mn	ICP-ES	µg/g	17880	17890	17520	12260	17110	9350
Mo	ICP-ES	µg/g	< 175	< 175	< 175	< 175	< 175	< 175
Na*	ICP-ES	µg/g	NA	NA	NA	NA	NA	NA
Nb	ICP-ES	µg/g	< 890	< 890	< 890	< 890	< 890	< 890
Nd	ICP-ES	µg/g	< 380	< 410	440	< 460	500	< 310
Ni*	ICP-ES	µg/g	NA	NA	NA	NA	NA	NA
P	ICP-ES	µg/g	3770	3680	4000	3370	3370	3200
Pb	ICP-ES	µg/g	5090	5080	5660	7240	6030	4510
Re	ICP-ES	µg/g	< 90	< 90	< 90	< 90	< 90	< 90
S	ICP-ES	µg/g	< 720	1530	< 650	1050	< 730	< 590
Si	ICP-ES	µg/g	9800	10500	9850	11900	12000	13400
Sn	ICP-ES	µg/g	< 450	< 450	< 450	< 450	< 450	< 450
Sr	ICP-ES	µg/g	20610	20450	20100	110	19250	70
Ti	ICP-ES	µg/g	620	630	600	1040	600	550
V	ICP-ES	µg/g	< 230	< 230	< 230	< 230	< 230	< 230
Zn	ICP-ES	µg/g	6520	6760	6390	9540	7330	6280
Zr	ICP-ES	µg/g	33000	32700	34200	33700	31900	32900

*Sodium and nickel data were unavailable due to an interference with the digestion method.

Solids Analysis - continued

Analyte	Method	Units	FB-13	FB-14
Ag	ICP-ES	µg/g	650	630
Al	ICP-ES	µg/g	120000	123000
B	ICP-ES	µg/g	1250	1480
Ba	ICP-ES	µg/g	210	470
Ca	ICP-ES	µg/g	4500	3840
Cd	ICP-ES	µg/g	34100	35900
Ce	ICP-ES	µg/g	< 1360	< 1250
Co	ICP-ES	µg/g	1570	1220
Cr	ICP-ES	µg/g	2300	2960
Cu	ICP-ES	µg/g	700	280
Fe	ICP-ES	µg/g	233000	248000
K	ICP-ES	µg/g	2900	4140
La	ICP-ES	µg/g	7430	7880
Li	ICP-ES	µg/g	< 175	< 175
Mg	ICP-ES	µg/g	2310	2090
Mn	ICP-ES	µg/g	20620	14610
Mo	ICP-ES	µg/g	< 175	< 175
Na*	ICP-ES	µg/g	NA	NA
Nb	ICP-ES	µg/g	< 890	< 890
Nd	ICP-ES	µg/g	< 470	< 430
Ni*	ICP-ES	µg/g	NA	NA
P	ICP-ES	µg/g	3530	3730
Pb	ICP-ES	µg/g	9130	6800
Re	ICP-ES	µg/g	< 90	< 90
S	ICP-ES	µg/g	1400	< 810
Si	ICP-ES	µg/g	13500	12800
Sn	ICP-ES	µg/g	< 450	< 450
Sr	ICP-ES	µg/g	19220	10050
Ti	ICP-ES	µg/g	1180	700
V	ICP-ES	µg/g	< 230	< 230
Zn	ICP-ES	µg/g	11070	7940
Zr	ICP-ES	µg/g	31300	31700

*Sodium and nickel data were unavailable due to an interference with the digestion method.

APPENDIX H.
X-RAY DIFFRACTIONS OF TEST SOLIDS

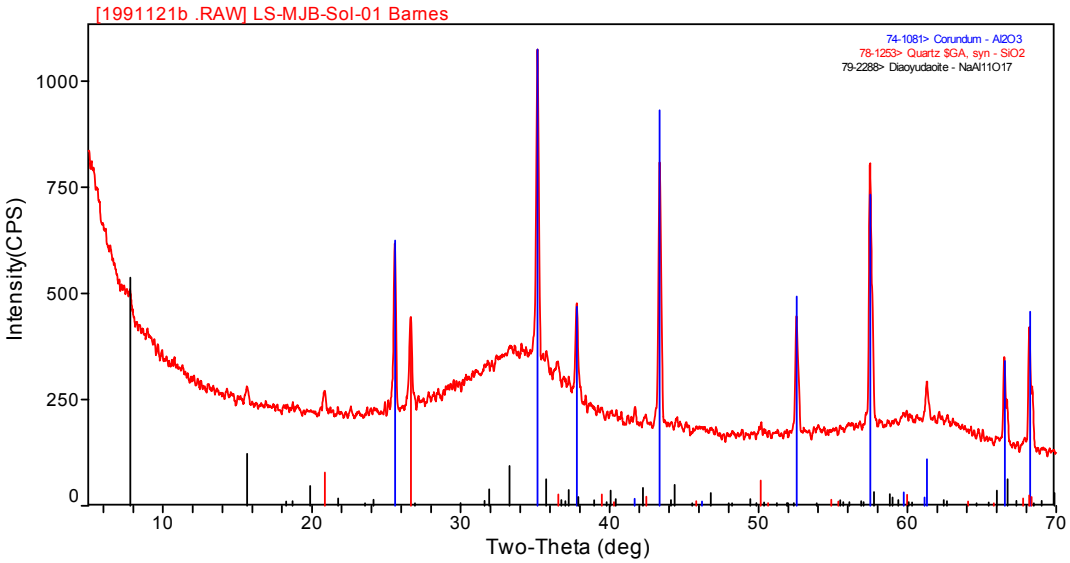

Figure H- 1. Test FB-01

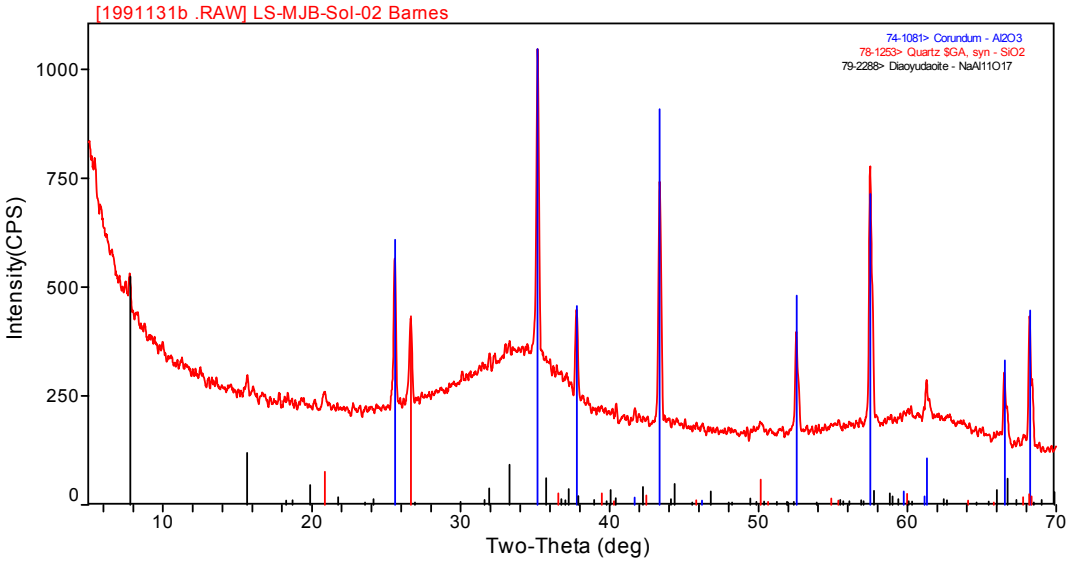

Figure H- 2. Test FB-02

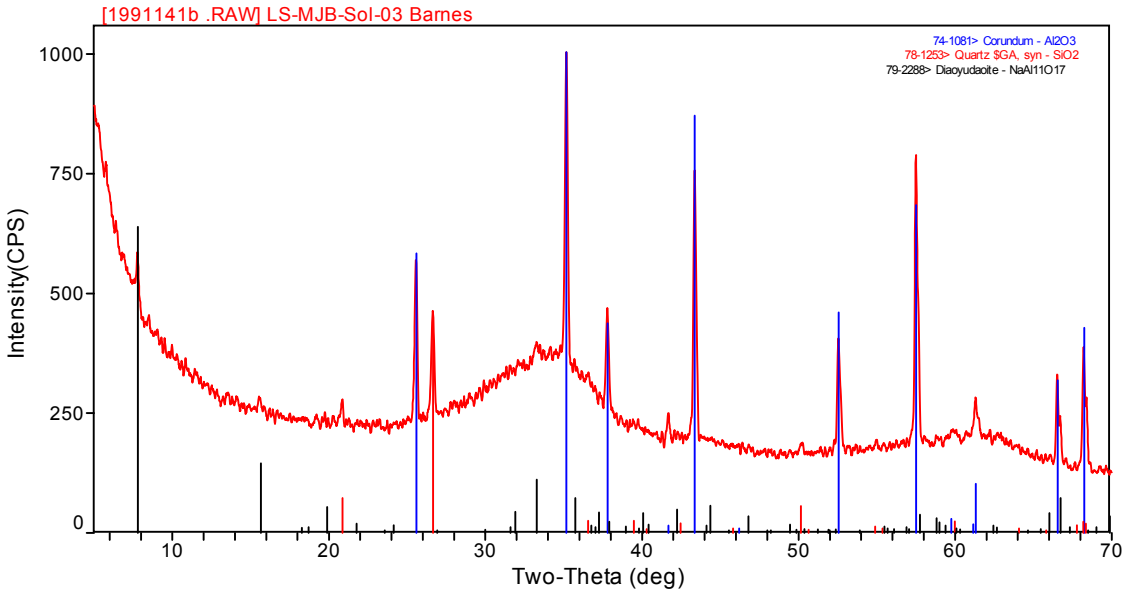

Figure H- 3. Test FB-03

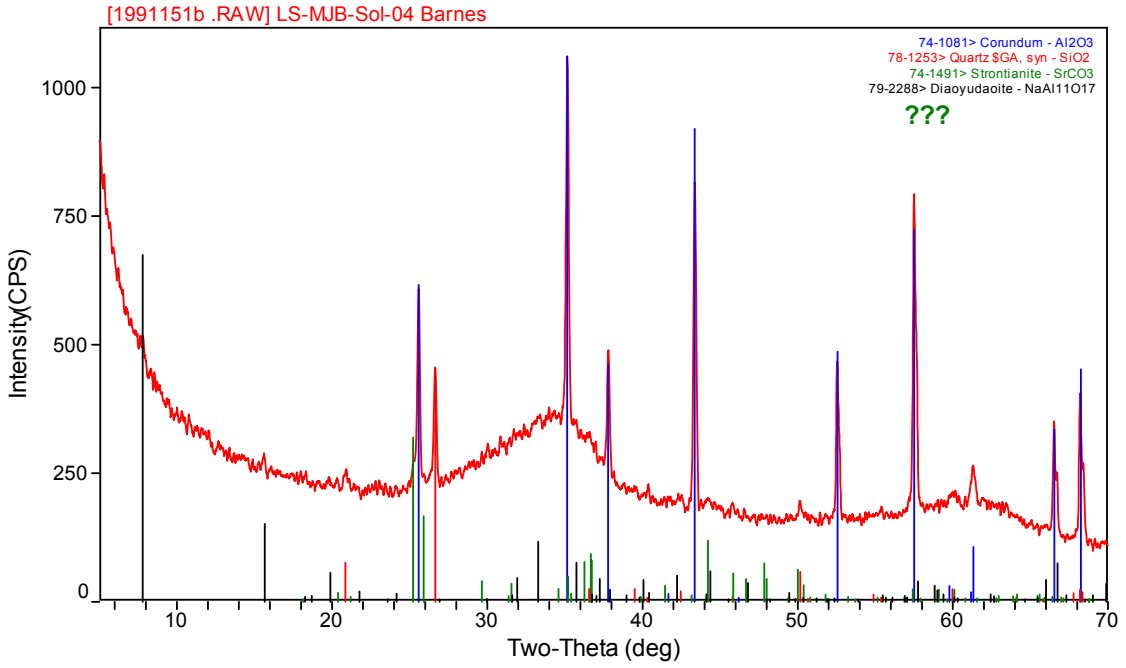

Figure H- 4. Test FB-04

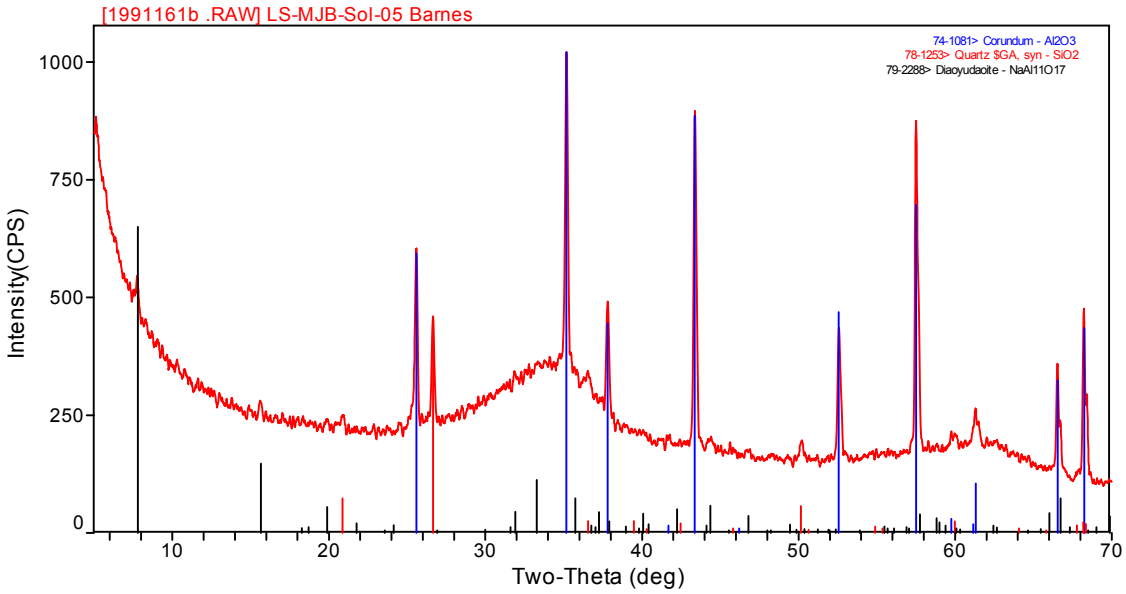

Figure H- 5. Test FB-05

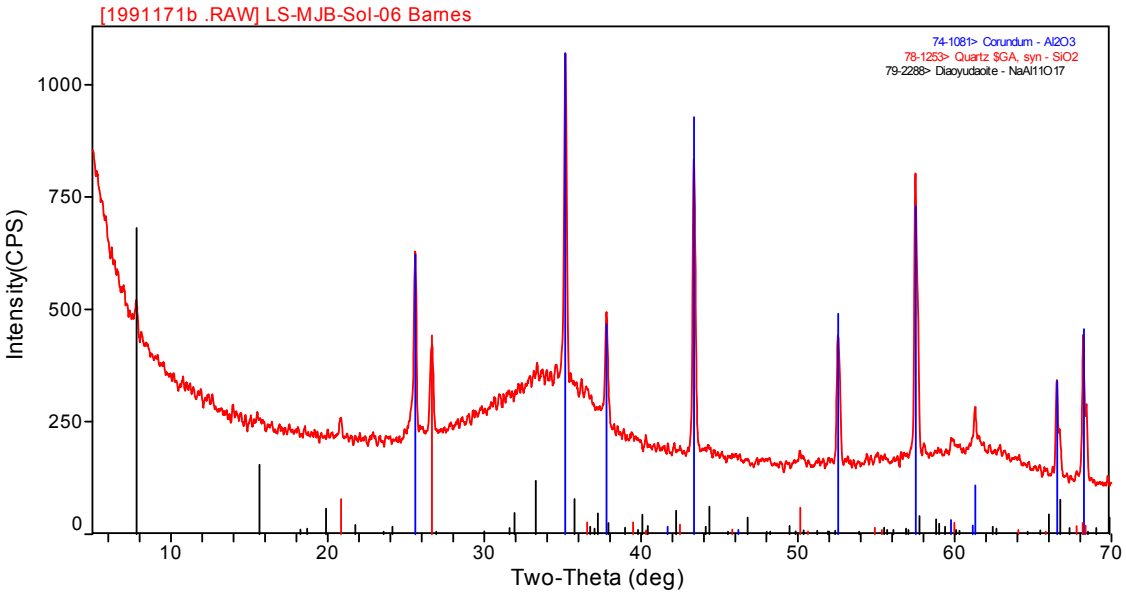

Figure H- 6. Test FB-06

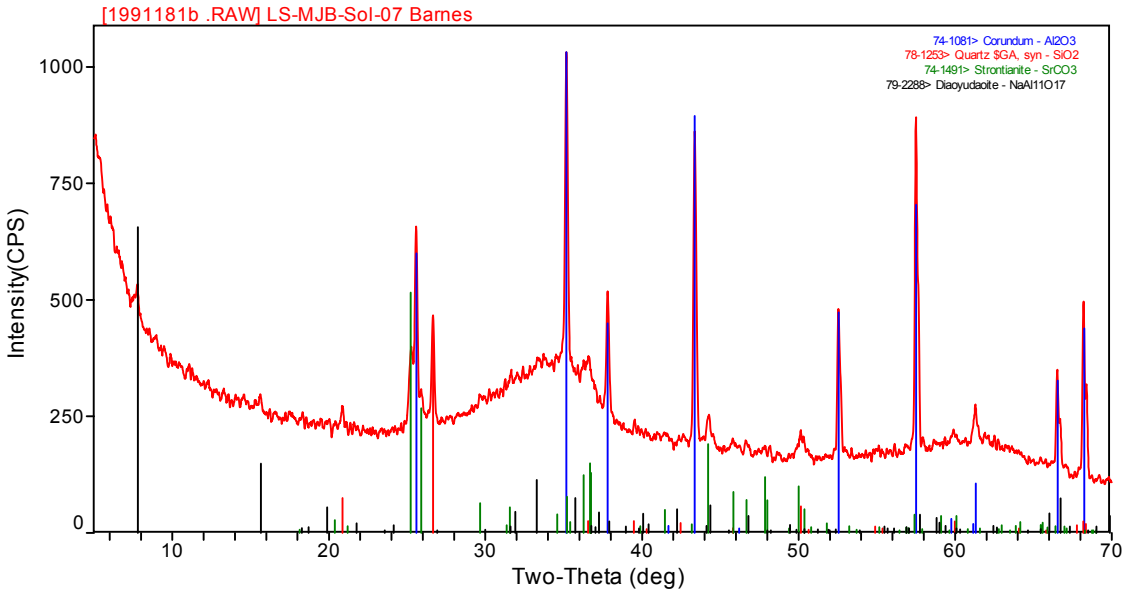

Figure H- 7. Test FB-07

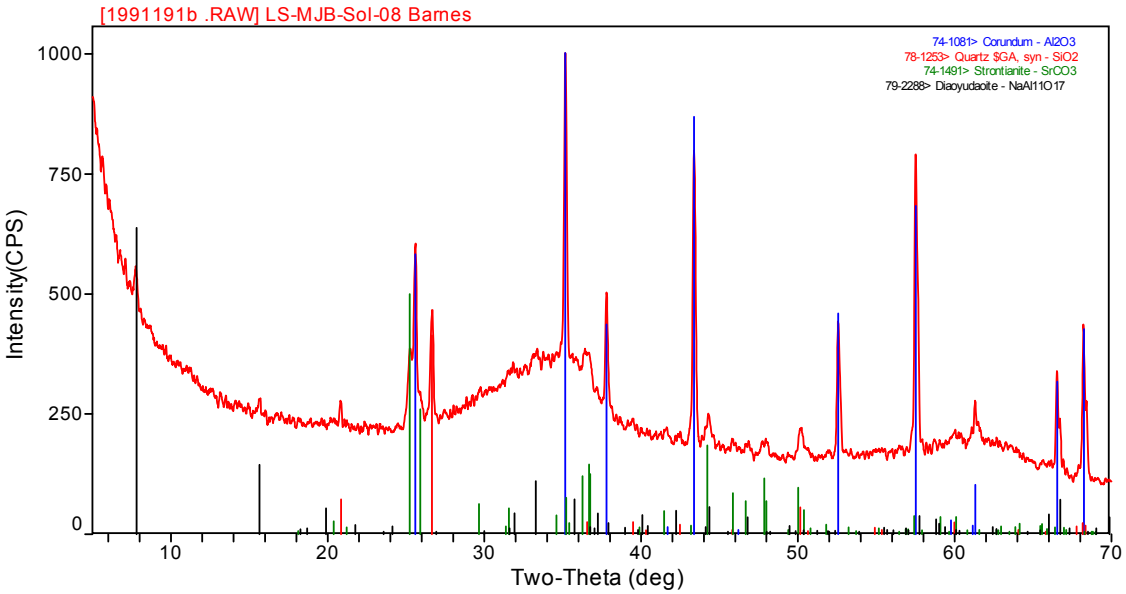

Figure H- 8. Test FB-08

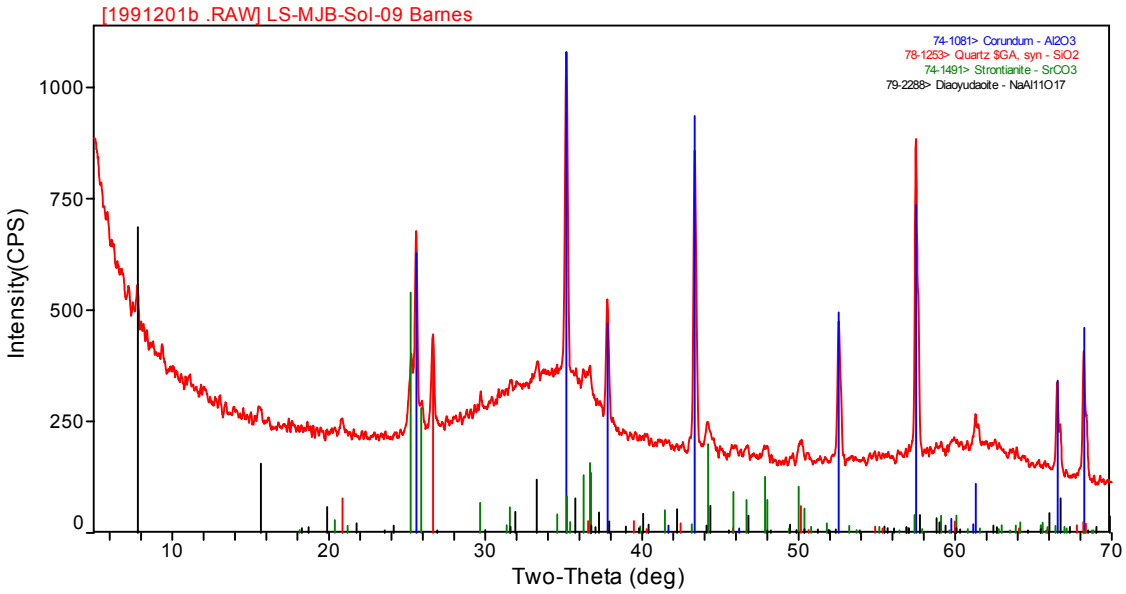

Figure H- 9. Test FB-09

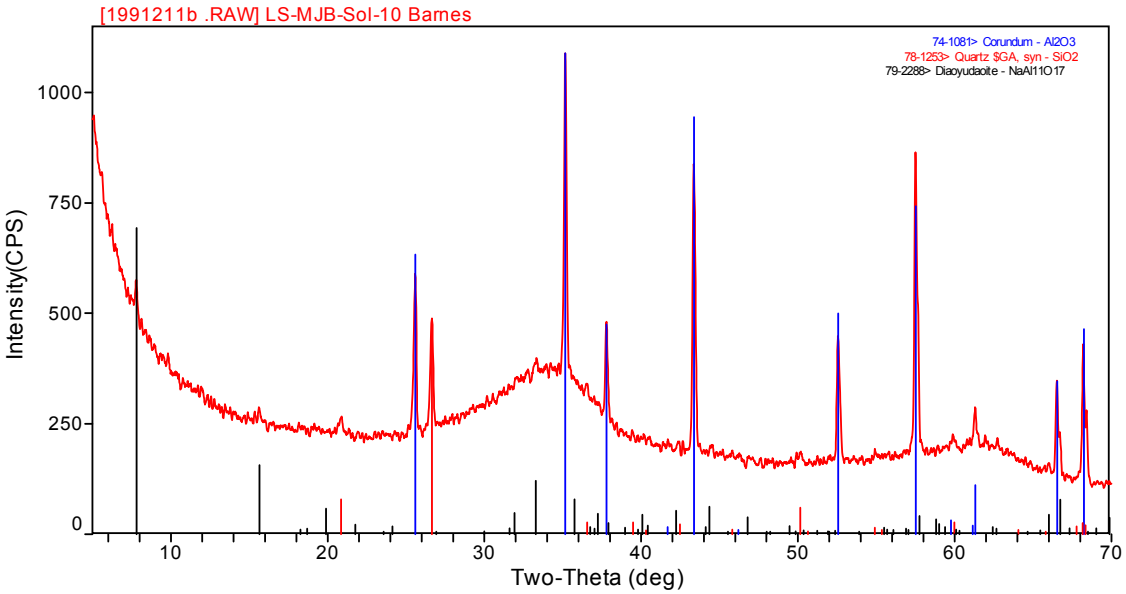

Figure H- 10. Test FB-10

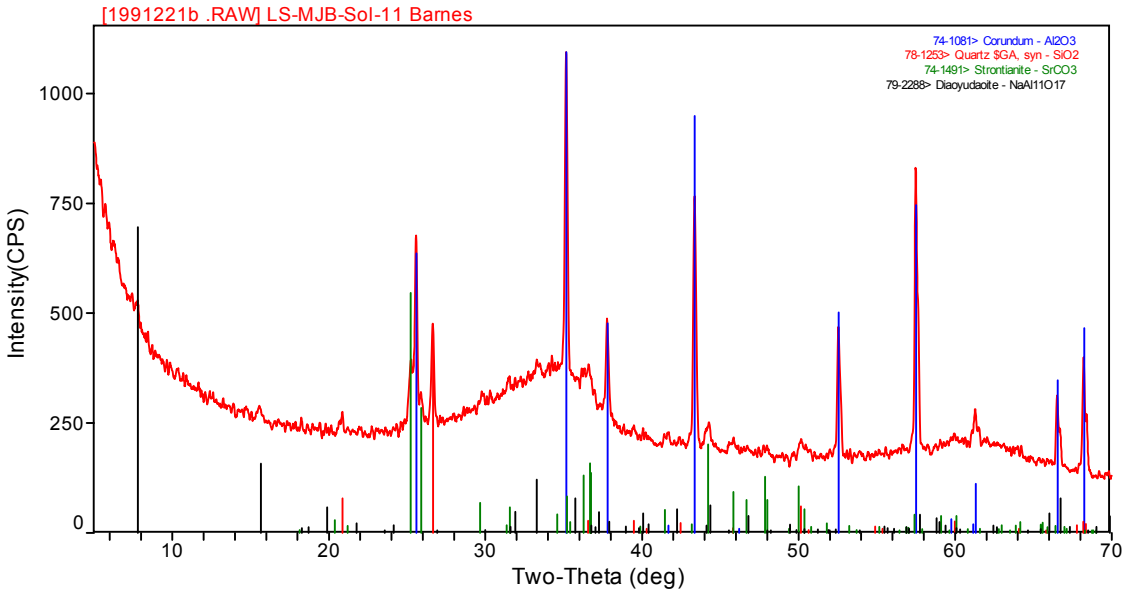

Figure H- 11. Test FB-11

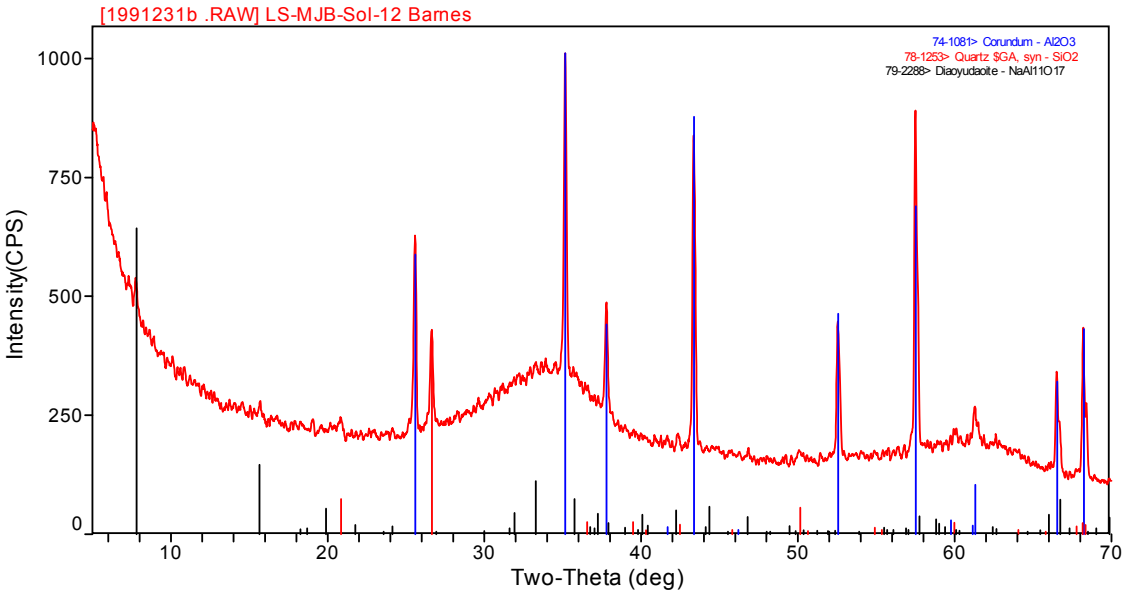

Figure H- 12. Test FB-12

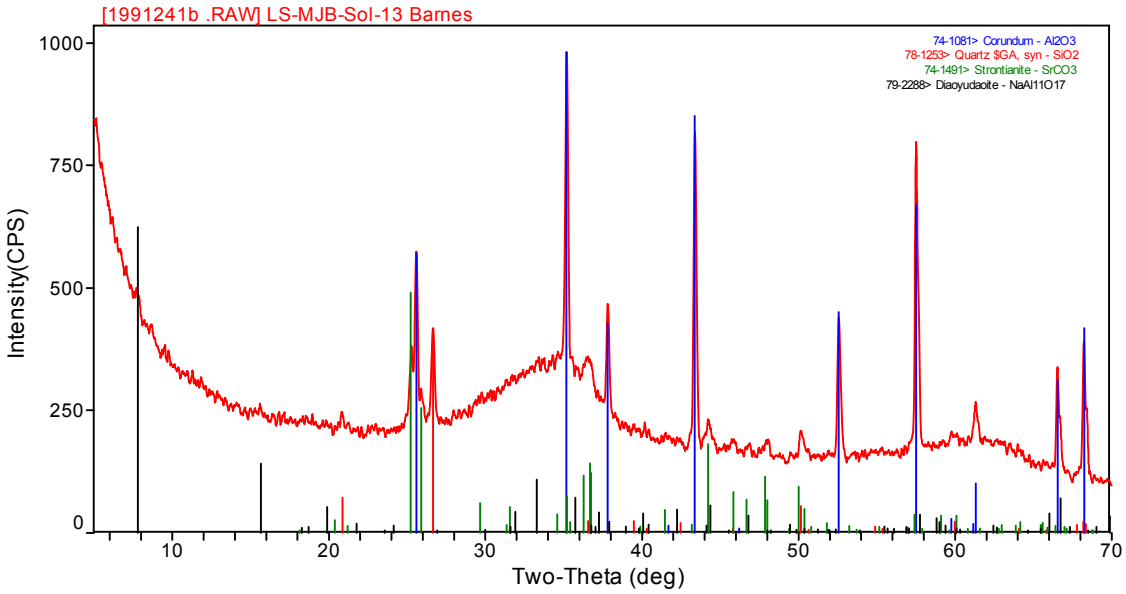

Figure H- 13. Test FB-13

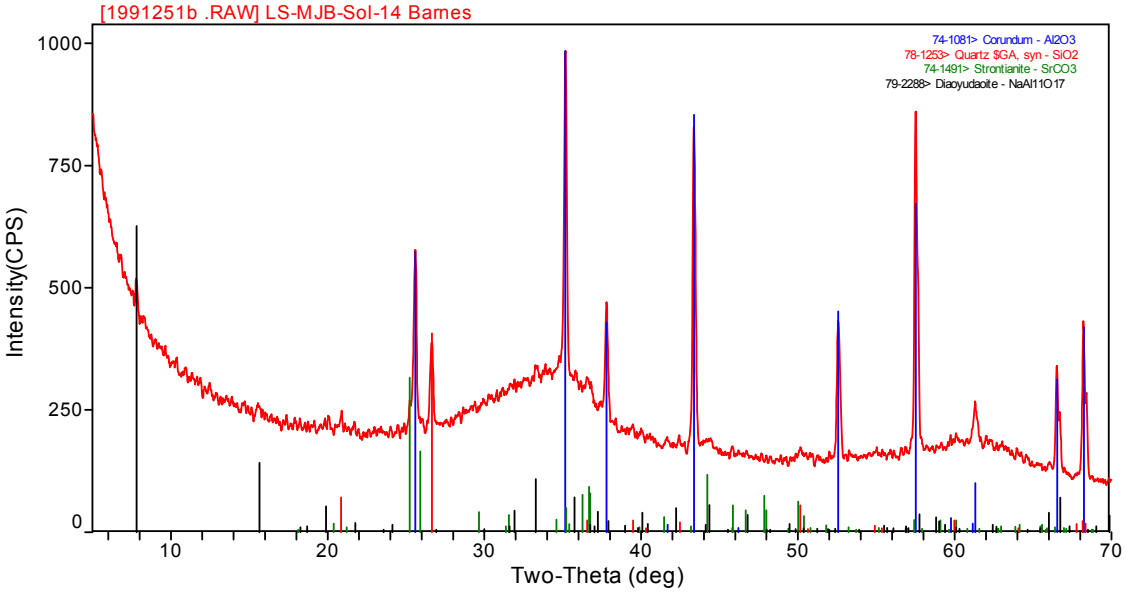

Figure H- 14. Test FB-14

This page intentionally left blank.

APPENDIX I.
STATISTICAL DESIGN ANALYSIS

Exhibit 1. Wt% Solids versus Experimental Factors and Groupings

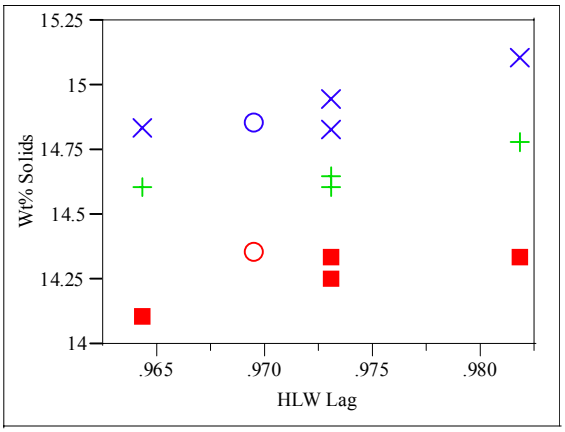

Wt% Solids By HLW Lag

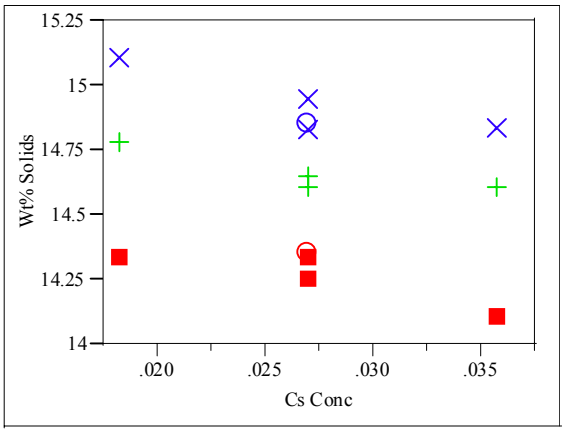

Wt% Solids By Cs Conc

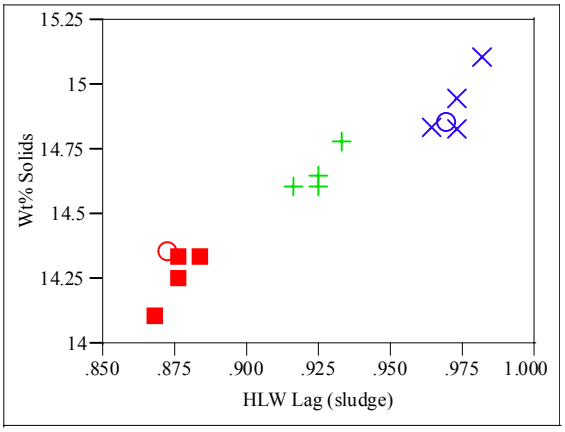

Wt% Solids By HLW Lag (sludge)

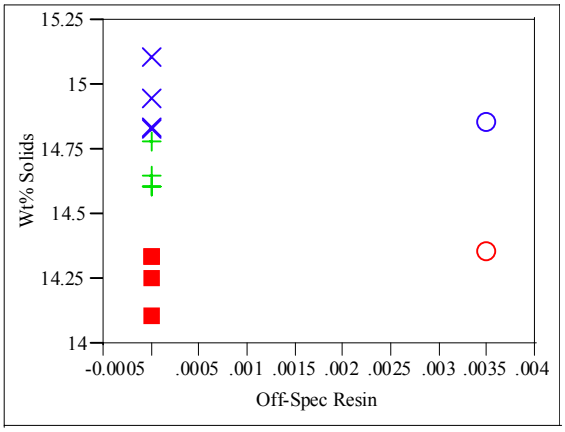

Wt% Solids By Off-Spec Resin

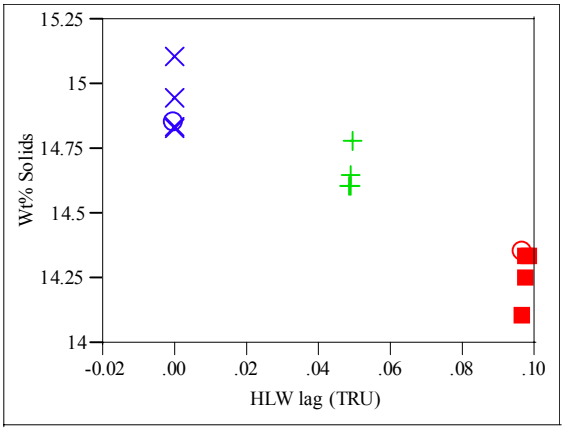

Wt% Solids By HLW lag (TRU)

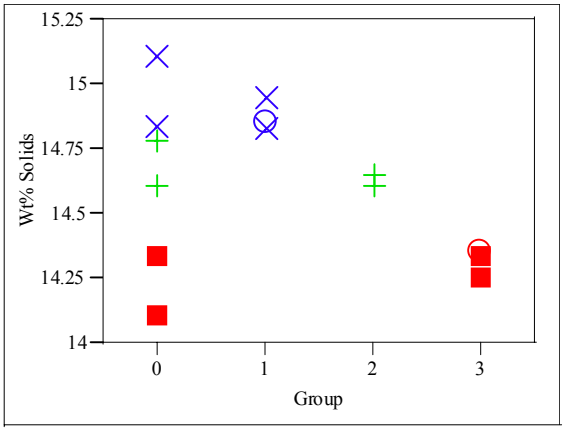

Wt% Solids By Group

Exhibit 2. Linear Mixture Model of Wt% Solids

Response Wt% Solids
Singularity Details
Intercept = 0
Whole Model

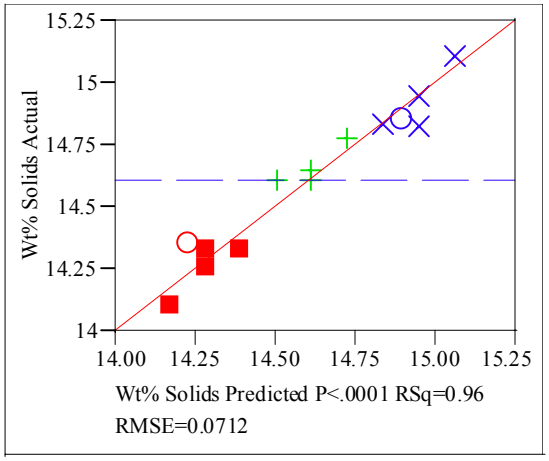

Actual by Predicted Plot

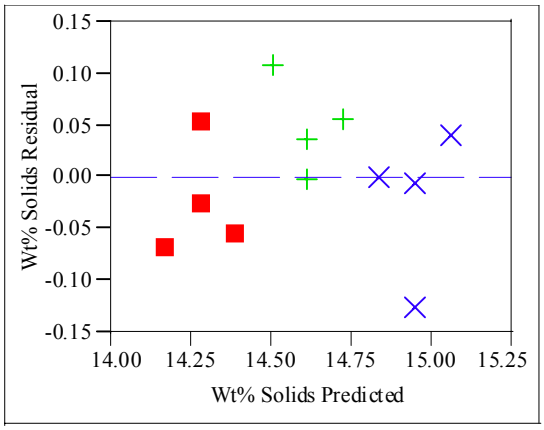

Residual by Predicted Plot

Summary of Fit

RSquare	0.955248
RSquare Adj	0.945303
Root Mean Square Error	0.071162
Mean of Response	14.6125
Observations (or Sum Wgts)	12

Analysis of Variance

Source	DF	Sum of Squares	Mean Square	F Ratio
Model	2	0.9728485	0.486424	96.0543
Error	9	0.0455765	0.005064	Prob > F
C. Total	11	1.0184250		<.0001

Lack of Fit

Source	DF	Sum of Squares	Mean Square	F Ratio
Lack Of Fit	6	0.03437649	0.005729	1.5347
Pure Error	3	0.01120000	0.003733	Prob > F
Total Error	9	0.04557649		0.3896
				Max RSq
				0.9890

Parameter Estimates

Term		Estimate
Intercept	Zeroed	0
HLW Lag (sludge)		15.300869
HLW lag (TRU)		8.4141874
Cs Conc		2.189869